- Text highlighted by [redacted] corresponds to the remarks from the first reviwer
- Text highlighted by [redacted] corresponds to the remarks from the second reviwer

The changes not being highlighted:

- The abstract has been improved
- English writing has been improved and odd usages removed
- More information have been added in the caption of the figures.

Reply to Reviewer 1

Review of manuscript ACP-2021-971

The manuscript presents results from the observation of two events of aged biomass burning aerosol over Lille (northern France) using a lidar with 3 elastic channels (1064 nm, 532 nm, and 355 nm), 2 Raman channels (the N_2 vibro-rotational channel at 387 nm and a purely rotational channel at 530 nm), which provide the capacity to measure aerosol extinction coefficient – and lidar ratio – without assumptions, 3 depolarization channels (1064 nm, 532 nm, and 355 nm) to measure linear particle depolarization ratio, and 1 fluorescence channel at 466 nm serving to identify the biomass. Other satellite observations, from CALIPSO and from Suomi NPP, as well as ground-based observations from AERONET Sun/sky photometers, are used as ancillary data.

The results permit to identify different properties of the aerosol in two case studies, which can be related to different wildfire source areas and/or aging processes.

General remarks

The study carried out is interesting and points toward new methods to characterize aerosols (not only biomass burning), but it looks a little inconclusive. Probably, it would benefit of being less ambitious in its scope and focusing on the question of the title, "what can a multi-wavelength Mie-Raman-polarization-fluorescence lidar provide?", which is, in my view, a little lost in rather inconclusive discussions on optical properties and on the possibility of biomass burning aerosols acting as ice nucleating particles. Not that these issues should not be dealt with, but probably with less detail, getting more to the facts, i.e. to what the measurements show. Because lidars with Raman channels and depolarization capabilities have long existed, I suggest that the paper focus more on the additional information provided by the fluorescence-measurement capability of the lidar used in the study.

Reply: Thanks a lot for the suggestions. The changes of BBA properties during the aging process and BBA acting as ice nucleating particles are very interesting topics, which fluorescence measurements could contribute to. We agree that the discussion about the smoke aging and ice nucleation is a bit too long and inconclusive. We need more observations, which are not presented in this manuscript, to consolidate them. An article more relevant to ice nucleation in smoke layer has been accepted by ACP. Therefore, we decided to follow the suggestion of the review, i.e. shorten the discussion about ice nucleation and focus more on the fluorescence measurements. The modifications can be seen in the new version of manuscript.

Specific remarks

1. Lines 141-142: the 530 nm Raman channel is described as "rotational Raman of nitrogen". However, it is unlikely that this channel picks up only lines from the nitrogen rotational Raman spectrum; most probably it also collects lines from the oxygen rotational Raman spectrum. Please check and correct if necessary.

Reply: Yes, the 530 nm channel includes the rotational spectrum of both nitrogen and oxygen. The manuscript has been modified.

2. Line 148: although for the lidar configuration and its capabilities the reader is referred to published references, I think that the less usual fluorescence capacity parameter would deserve an explicit definition in the text. Probably it would fit right after "fluorescence capacity" in line 148.

Reply: Two equations are added to define fluorescence backscattering coefficient and fluorescence capacity. We also added some examples of fluorescence and non-fluorescence aerosols in the manuscript.

3. Line 184 and figure 7(c): there seems to be some undefinition as to what is represented in figure 7. The text (line 184) says that it shows the "relative fluorescence signal $\frac{P_{387}}{P_{466}}$, First of all, in case it is this ratio what is represented, please specify if this ratio is calibrated. Second, the caption of figure 7 says that what is represented is the backscatter coefficient of fluorescence at 466 nm, which is not quite the ratio given in line 184. Check as well the caption of fig. 9.

Change the caption.

4. Lines 185-186: strong depolarization seems to be unambiguously ascribed to the presence of ice particles ("Ice particles with strong depolarization were detected within the smoke layers above 8000 m"). My first remark is that a call to the figure showing that (figure 7(b)?) is missing; the period of time when the strong depolarization is observed should also be specified. Secondly, this strong depolarization seems to come from cirrus clouds. It is known that depolarization can also be produced by multiple scattering. Can multiple scattering be ruled out as the cause of depolarization in this case? What's the lidar field of view? Even if the presence of ice is plausible, I think that the evidence for ice being the cause of depolarization should be developed further.

Reply: (1) Reference to Figure 7(b) is added. (2) Indeed, it is not accurate to say that the increases of volume depolarization ratio at above 8000 m are all caused by the presence of ice particles, because some variations are aparently due to the fluctuation of BBA concentrations. To be more accurate, the sentence is changed to "Ice particle featured with increased depolarization ratios were detected in some high BBA layers, e.g at 8000-1000 m at 17:00-18:00 UTC ". Multiple scattering can be excluded for causing high depolarization ratios in the smoke layer, because firstly the lidar field of view is small, i.e. 1 mrad, and secondly in this case, the concentration of BBA was too low to produce so strong multiple scattering effect.

5. Line 205: "Figure 8(g) presents the WVMR, RH and temperature profiles". However, figure 8(g) doesn't seem to contain a temperature profile.

Reply: It was a mistake. The temperature profile is plotted in Figure 8(d). The caption of the figure and the text are corrected now.

6. Lines 209-210: Talking about figure 8(g), it is said that "The WVMR increases from the plume center to the edge, suggesting that the WVMR is an important role in the aging process." I don't see that increase in the WVMR profile in figure 8(g), rather that profile follows the profiles of β and β_F.

Reply: The sentence quoted was not well written. I wanted to express that the WVMR in the core of BBA plume, i.e. 5000-6000 m, was higher than at the edge 7000-9000 m. The sentence is rewritten as follows:

"The WVMR in the core of the plume is obviously higher than at the plume edge, suggesting that the WVMR is a potential indicator and/or factor in the aging process."

7. Line 231: "A sharp increase of $PLDR_{1064}$ to nearly 0.10 was detected at 8600 m, indicating the presence of ice crystals". Two remarks: a) Where should the reader look for that sharp increase? b) See my second remark in point 4.

Reply: Reference to Figure 10(e) has been added.

8. Line 275: "The vertical variation of lidar ratios are also obvious in September (Figure 5)". First, it's unnecessary to talk about September, as all the presented measurements were carried out in September. Second, I don't see that fig. 5(a) makes obvious that variation. Although a variation in the lidar ratios can be seen between periods P1-P6 and periods P7-P9, I don't see that this variation is related to some vertical variation. For example, in period P2 the BBA layer is detected between 5500 and 8500 m, and in period P7, with lower lidar ratio, between 5400 and 8500 m, which is sensibly the same range as for P2. Please check if the figure referred to should be figure 5 or else be more explicit about what the reader should pay attention to.

Reply: (1) 'September removed'. (2) Yes, it shoud be Figure 5. The statistics shown in Figure 5 are taken from the plumes observed in different time interval. It means that, for one time interval, the data points in the box plot are simultaneously presented at consecutive vertical levels. And the vertical variations are reflected by the height of the boxes. In Figure 5(a), the vertical variations of lidar ratios are important, especially in P3 and P4. For example, in P4, LR_{532} varied from about 52 sr to 90 sr at 5500-7500 m.

9. Line 279: "From this aspect, the fluorescence capacity is a better parameter for aerosol typing especially in low aerosol concentrations". Please be more specific as to the meaning of "typing" in this context.

Reply: Typing means classification, to classify aerosol types into different categories, such as pollen, dust, smoke and so on.

Formal remarks and typos

1. In the bibliography, please insert the doi whenever possible.

   Reply: doi numbers are now added to the bibliography.

2. As a general rule, I would prefer that the full wording of acronym is used before the acronym; for example, in line 68, I would prefer "showed enhanced particle linear depolarization ratios (PDLRs)" than the current "showed enhanced PLDRs (particle linear depolarization ratio)".

   Reply: corrected

3. Line 31: "They could alternate the planetary radiation budget of the planet". I think that the meaning is "They could alter the radiation budget of the planet".

   Reply: Yes, it should be alter.

4. Lines 80-81: "could influence the ability in water diffusion". This sentence sounds strange. Should it be "could influence the ability for water diffusion", or there is a word missing? Please check.

Reply: Yes, “the ability of water diffusion” is better.

5. Lines 96-97: ATOLL is defined (Atmospheric Observatory of LiLle), but is never used afterwards.

   Reply: Yes, after correction, ATOLL, instead of Lille, is refered when mentioning the lidar site.

6. Figs. 1(c) and 2 are not cited in the text. Also, the text where the call to figure 2 should be inserted (section 2.2) comes after the call to figure 3 in section 2.1, so the numbering of these figures should be swapped.

   Reply: corrected

7. Line 162: “and the height range of the layers are resented”. “resented” should be “presented”.

   Reply: corrected

8. Line 162: please insert the acronym LR after the lidar ratio is introduced, e.g. “Lidar ratio (LR), i.e. the ratio between extinction coefficient and backscatter coefficient”.

   Reply: corrected

9. Lines 171-173: “Apart from the temporal variations, vertical variations in the BBA layers are also significant, such as lidar ratios in on 12 and 14 September, PLDRs on 11 and 18 September. Such variations are possibly indications of the variabilities in the burning materials, combustion conditions and aging process”. Where are these lidar ratios and PLDRs represented? Where the reader should look at?

   Reply: The vertical variations in the BBA layers, indicated by the distance between the bottom and the top of each box plot in Figure 5, are also significant, such as lidar ratios in on 12 and 14 September, the PLDRs on 11 and 18 September.

10. Lines 188-189: “Figure 8 plots the parameters obtained from averaged observations between 22:00 UTC, 11 September and 03:00 UTC, 12 September”. However, the caption of figure 8 says that the averaging end time is 02:00 UTC.

    Reply: Corrected. The caption was mistaken, it should be 03:00 UTC.

11. Line 197: “The increasing trend”. Should it be “decreasing”? (see the sentence just before and fig. 8).

    Reply: Corrected. It should be “decreasing”.

12. Line 205: Although evident for the expert, the acronyms WVMR and RH have not been defined.

    Reply: Definitions are added at the places where the two acronyms first appear.

13. Line 253: “episode of Canadian smoke over Europe”. Please insert references, even if it implies repeating some of those already given in line 251.

    Reply: References added.

14. As general rule, increase the size of legends, labels and scales in the graphs. Be also explicit in the labels. For example, the label of the color bar of figure 4(b) should read “Volume depolarization ratio at 1064 nm” instead of “VDR_1064_AN”. I don’t know if specifying that measurements are obtained from analogue (AN) or photon counting (PC) channels is relevant in the context of this paper.

    Reply: The size of the labels have been increased. ‘AN’ and ‘PC’ are indeed unnecessary information and have been removed.

15. Figure 2: the labels (a) and (b) are missing in the figure panels.

    Reply：labels are added.

16. Figure 5. Please explain that P1, P2,...P9 in the horizontal scales refer to the periods identified in table 1.

    Reply：The explanation has been added.

17. Figure 5 caption, 3rd line: “The dot and bar in the box indicate the mean value and the middle value”. “middle value” should probably be “median value”.

    Reply：Corrected.

18. Although the English writing is very good in general, I would suggest a review by a native English speaker to fix some odd uses. Just as an example, in lines 12-13, the “varied” in the sentence “It reflects that the properties of aged BBA particles are highly varied” should probably be “variable”; in line 15 “than those” sounds better than “with those”, etc.

    Reply：English writing has been improved.

Reply to Review #2

by Qiaoyun HU

The paper discusses interesting measurements of aged biomass burning smoke with a unique lidar. The paper is well written and appropriate for ACP. The measurements are performed with a recently introduced advanced lidar that combines multiwavelength lidar, Raman lidar, polarization lidar, and (new!) fluorescence lidar techniques.

Minor revisions are necessary.

p3, l75: When discussing INP, please keep in mind that these aged smoke particles are organic aerosol particles, the organic properties (of humic-like substances) count, and not the ones for soot or fly ash. Therefore, Knopf et al. 2018 .... is appropriate as reference.

1. Knopf, D. A., Alpert, P. A., and Wang, B.: The role of organic aerosol in atmospheric ice nucleation: a review, ACS Earth and Space Chemistry, 2, 168–202, https://doi.org/10.1021/acsearthspacechem.7b00120, 2018.

   Reply: added.

2. p4, l96: One may cite Baars et al., 2021: Baars, H., et al. (2021). Californian wildfire smoke over Europe: A first example of the aerosol observing capabilities of Aeolus compared to ground-based lidar. Geophysical Research Letters, 48, e2020GL092194. https://doi.org/10.1029/2020GL092194

   Reply: added.

3. p4, l105: Please use 'pyroCb' instead of 'pyCb'!

   Reply: Corrected.

4. p4, l112: Figure 1(b) is mentioned, and then (l114) Figure 3 is mentioned. Figure 2 is left out.

   Reply: The order of Figure 2 and 3 is swapped.

5. P5, l126: No one should introduce Figure 2!

   Reply: Reference to Figure 2 added.

6. p5, l128: AE decreased...

   Reply: Corrected. Yes, AE decreased.

p5, l133: To my understanding, Cimel (AERONET) is unable to correctly measure AODs>4.0. And now we have peak AODs of 5.8!

Reply: The new photometer is able to measure AOD up to 7.0. The AOD of 5.8 remains in the Level 2 data, which means it has been validated.

The Case study section is a bit boring, one should better emphasize the deviation of the optical properties on 17-18 Sep 2020 in Figure 5 from the rest, to make the entire story more exciting.

Reply: The presentation of case studies is now modified in the following ways:

1. In the Case 1, the introduction of BBA characteristics is kept and simplified.

2. In Case 2, the differences of BBA characteristics compared to Case 1 are emphasized.

So the repetition of numbers is avoided and the comparison of BBA properties is more clear.

Section 4: Discussion

I miss a clear structure of this section. The discussion could be shortened and should clearly highlight the added value now available in terms of the fluorescence information. Please state clearly: What is new! The discussion should be some kind of a review of the recent Veselovskii papers 2020 (general method), 2021 (on pollen) and the recent one on smoke/cirrus observations (also submitted in 2021) together with the present article on North American smoke.

I would leave out any speculation. For example, the discussion on age of smoke as a function of height. This is just speculation, and usually depends on many different factors such meteorological conditions, fire type, burning material, size of burning area and so on....).

Some suggestions that should be considered. The smoke particles are usually glassy in the upper troposphere and stratosphere (see the review article of Knopf et al.) The organic coating means that the INP properties are controlled by organic (humic-like) material. When discussing heterogeneous ice formation, do not restrict yourself to mixed phase clouds and temperatures higher than -35C. Heterogeneous ice nucleation also occurs at -50 to -70C (in cirrus). All this should be mentioned.

Furthermore, PLDR (or better, ... the shape properties) seem to depend on relative humidity (availability of water vapor) and further gases that can condense on smoke

particles to make them spherical. And the concentration of the gases are high in the lower troposphere and then obviously decrease with height from the middle to the dry upper troposphere and the extremely dry stratosphere.

page 9, line 267-274: I would leave out such a discussion.

Reply: The discussion has been condensed and restructured in the following ways:

1. Speculations and unnecessary discussions about modeling are removed.

2. Section 4.1 and 4.2 merged.

3. The discussion about smoke acting as INP shortened and condensed.

4. The discussion is organized in four paragraphs, each with one different topic: PLDR, lidar ratio, aerosol fluorescence and smoke acting as INP.

page 9, line 275-280, please state clearly how you calculate the lidar ratio, You cannot combine extinction and backscatter values obtained with DIFFERENT smoothing lengths.

Reply: After checking the code of lidar data processing, I confirm that the smoothing length for extinction and backscatter profiles is the same ! I forgot that I had considered the possible artifacts of using different smoothing length when developping the code longtime ago, so the statement in the manuscript was wrong and it has been removed. Thanks a lot for this remark !

page 9, line 287 to page 10, line 297: I would leave this discussion out as well. The paper deals with fluorescence. Please clearly state what is new...! Provide clear facts, what the added value is!

An extra section 4.2 on BBA as INP is not needed in this fluorescence-related paper. A paragraph on the impact of smoke serving as INP is sufficient, but please cover the full range of clouds from mixed phase clouds to cirrus (-25C to -70C), and then a reference to the recent Veselovskii paper on smoke-cirrus interaction is needed.

Veselovskii, I., Hu, Q., Ansmann, A., Goloub, P., Podvin, T., and Korenskiy, M.: Fluorescence lidar observations of wildfire smoke inside cirrus: A contribution to smoke-cirrus – interaction research, Atmos. Chem. Phys. Discuss. [preprint], https://doi.org/10.5194/acp-2021-1017, in review, 2021.

Reply: Section 4.1 and 4.2 have been merged.

The conclusion section should finally also be better organized and structured. I do not agree that the fluorescence information is the better information to identify

smoke. It is an additional one, more precise, another independent one, besides all the useful information on PLDR spectrum and lidar ratio spectrum.

Reply: The conclusion section has been re-organized. The sentence--"the fluorescence information is the better information to identify smoke" is ambiguous and has been removed from the conclusion and elsewhere. We want to emphasize that the fluorescence is very sensitive and is accessible even at low aerosol concentration and high altitude, while the calculation of lidar ratio requires smooth and at least moderate concentration of aerosols. But for sure the fluorescence is a supplementary information and should not replace extinction or backscattering measurements.

Figure 3: mixed-phase cloud at 10 km height? Impossible!

Reply: This mixed phase cloud was detected in a subtropical region at (37.91N, 85.41W) by CALIPSO. The temperature at this altitude was roughly about -40 degrees, but the uncertainty could be large and the occurrence of super-cooled liquid water is still possible. In Lille (50.6N, 3.1E), we observed supercooled liquid water clouds at 8 km height and mixed phase clouds at higher altitudes in September. The appearance of ice crystals can be confirmed with the depolarization ratio of 0.2--0.4. These ice crystals appeared in a smoke layer and were possibly initiated by smoke particles. But the nucleation pathway cannot be revolved with the information we currently have and CALIPSO did not observed any mixed phase cloud. So I decided to changed "mixed phase cloud" into "ice crystals mixed with BBA" in order to avoid inaccurate expression.

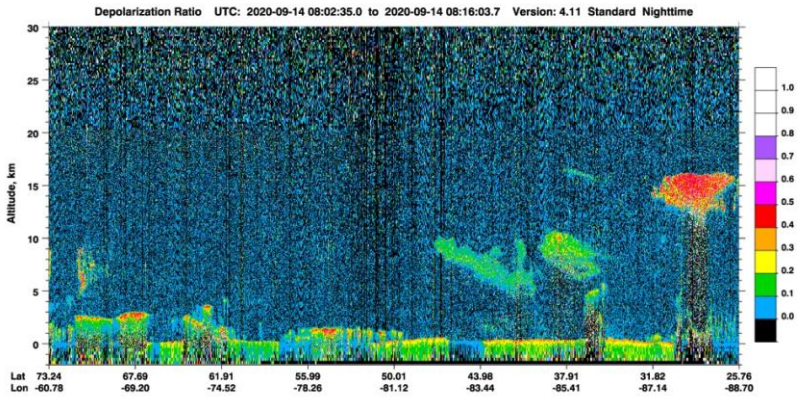

Fig 1. The depolarization ratio at 532 nm, CALIPSO measurements on 14-09-2020

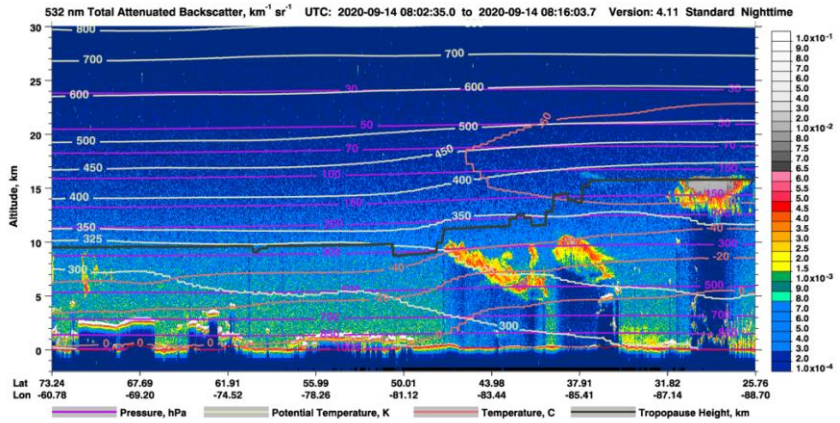

Fig 2. The total attenuated backscatter at 532 nm, CALIPSO measurements on 14-09-2020 overlaid with temperature and potential temperature.

Figure 4: All axis text must be enlarged, … is much too small at the moment.

Reply: Label size increased

Figure 5: (d) Y-axis EAE/BAE is confusing, better write …. EAE, BAE. In the caption, please explain explicitly which intense parameters are shown. What does P1-P9 mean? Please state that P1-P9 are listed in Table 1….

Reply: Corrected.

Figure 7: Again, all axis text must be enlarged, much too small at the moment.

Reply: Ticks are enlarged.

Figure 8: I would recommend to explain clearly what parameters are shown. Figures should be widely self-explaining.

Reply: More explanations have been added.

Figure 9: Again, all axis text must be enlarged, much too small at the moment.

Reply: Axis ticks are enlarged.

Figure 10: Here one could then state: Same as Figure 8, except…..

Reply: Caption updated.

Figure 11: Again, what is shown… should be stated.

Reply: Caption updated.

Regarding all the figures, keep in mind that many readers may not be lidar specialists and need a lot of information.

Reply: More information has been added in the caption of figures.

The characterization of long-range transported North American biomass burning plumes: what can a multi-wavelength Mie-Raman-polarization-fluorescence lidar provide?

Qiaoyun Hu[1], Philippe Goloub[1], Igor Veselovskii[2], and Thierry Podvin[1]

[1]Univ. Lille, CNRS, UMR 8518 - LOA - Laboratoire d'Optique Atmosphérique, F-59650 Lille, France
[2]Prokhorov General Physics Institute of the Russian Academy of Sciences, Moscow, Russia

Correspondence: Qiaoyun Hu (qiaoyun.hu@univ-lille.fr)

Abstract. This article presents a study of long-range transported biomass burning aerosols (BBA) originated from the North American wildfires in September 2020. The BBA plumes presented in this study were in the troposphere and underwent 1-2 weeks aging before arriving at the lidar station ATOLL (ATmospheric Observatory of LiLle) in northern France. A novel lidar-derived dataset, 2α+3β+3δ+ϕ (α: extinction coefficient, β: backscatter coefficient, δ: particle linear depolarization ratio, i.e., PLDR, ϕ: fluorescence capacity), is provided for the characterization of BBA. The fluorescence capacity is an intensive aerosol parameter describing the ability of aerosols in producing fluorescence when exposed to UV excitation. In our BBA observations, obvious variations in aerosol intensive parameters, reflecting the variability of BBA properties, were detected. The PLDRs varied from less than 0.03 at all wavelengths, to 0.15-0.22 and 0.12-0.16, respectively at 355 and 532 nm. The extinction related Angström exponent was within the range of -0.3 –1.0 and the fluorescence capacity was 1.0×10^{-4}– 4.0×10^{-4}. Lidar ratio as low as 24$\pm$4 sr (50$\pm$8 sr) was observed in the BBA plumes at 355 (532) nm on 17-18 September, which was lower than most previously observed aged BBAs. These variations are likely correlated with the combustion process, the lifting of BBA plumes and the conditions (temperature, humidities, etc.) in the aging process. In addition, our results indicate BBA could act as ice nucleating particles in tropospheric conditions. The lidar fluorescence channel proves to be an important added value in aerosol characterization and aerosol-cloud interactions studies, due to its high sensitivity. With the increase of wildfires occurrence and intensity, BBAs become a more and more important atmospheric component. In this context, we show the potential of our novel lidar-derived dataset for aged BBA particles characterization and for the understanding of their role in cloud processes.

1 Introduction

Severe wildfires caught the attention of the public and the scientific communities in recent years. Wildfires in North America increase in both frequency and intensity, due to the warming-up of the climate. Regarding the global scale, the duration of fire seasons increased by about 19% from 1979 to 2013 (Jolly et al., 2015; Schoennagel et al., 2017). Wildfires can directly impact the vegetation of earth's surface, the fertility of soils, water cycle and human society (Santín and Doerr, 2016; Ditas et al., 2018; May et al., 2014; O'Dell et al., 2020). Copious amount of fire emissions, including gases and particles, were injected into the

troposphere and occasionally into the upper troposphere and lower stratosphere (UTLS). Those emissions pose threats to the air quality and human health, because they contain mainly fine particles and some chemical compounds in wildfire emissions are toxic. They could alter the planetary radiation budget of the planet by scattering and absorbing the incoming solar radiation and influence the cloud process by modifying cloud properties and acting as INP (ice nucleation particle) and CCN (cloud condensation nuclei).

Wildfire emissions are composed of a mixture of gases, e.g. carbon monoxide, polycyclic aromatic hydrocarbons (PAHs) containing gas-phase hazardous air pollutants, water vapor and aerosol particles, such as black carbon (BC), organic carbon (OC), etc. In addition, water soluble ions (potassium, halides, sulfates) can also be produced by the decomposition of biomass and the subsequent condensation in the smoke plume. The OC components account for a substantial fraction, about 20% to 90% in wildfire emissions, much higher than BC. Humic-like substances, which are a complex group of high molecular weight organic compounds, contribute considerably to the mass of organic compounds and influence the light absorbing properties of aerosols (Urbanski et al., 2008; Santín and Doerr, 2016; Wu et al., 2018). For convenience, we use hereafter BBA (biomass burning aerosols) to refer to the aerosols resulting from wildfire emissions. Due to the complexity in the burning and the aging processes, the BBA properties are highly variable. The initial composition and size distribution of BBAs depend on the burning materials (i.e vegetation type, such as grassland, boreal forest, etc.) and environmental conditions (temperature, moisture, soil properties, etc.), which impact the combustion efficiency and the burning processes (i.e. flaming and smoldering). The smoldering phase, which is with lower temperature, could lead to a substantially higher conversion of burning materials to toxic compounds than the flaming phase, and produce more weakly absorbing OC aerosols. Fire emissions from high temperatures and the flaming phase tend to contain an increased proportion of BC to OC and have smaller smoke particles (Reid et al., 2005; Garofalo et al., 2019).

Fresh BBAs are fractal like aggregates of BC cores and OC coatings (China et al., 2013, 2015). During long-range transport, BBAs undergo complex aging processes, including condensation, oxidation, evaporation, coagulation, compaction, humidification and so on. These processes could modify the particles' morphology, composition, optical and chemical properties and hygroscopic properties. The aging process of wildfire emissions is not yet adequately characterized. It includes a complex group of chemical reactions and physical changes, among which the gas-to-particle condensation driven by oxidation and evaporation driven by aerosol dilution, are two important and competing processes. The oxidation process can produce more organic matter with lower volatility, while it could also lead to increased volatile SOA (secondary organic aerosol) due to fragmentation of some macromolecules. The evaporation tends to decrease the partitioning of OC aerosols as dilution shifts the gas-particle equilibrium more to the gas end. Measurements in laboratories and field campaigns do not reach a consensus on the relative balance of the two competing processes as they are controlled by many factors, such as the dilution rate, exposure to oxidants (O3, OH radical), travel time and so on. The growth of particle size is found in both near-field and longtime aged BBAs, while the causes might not be the same. Condensational growth is the dominating factor in fresh and near-field BBAs, while coagulational growth is dominating in aged BBAs. Abel et al. (2003) reported an increase of SSA (single scattering albedo) from about 0.84 to 0.90 in 5 hours after the emission, which is likely due to the condensation of scattering organic components on absorbing soot particles during early-stage aging. Similar changes in SSA are derived by Kleinman et al. (2020) when

investigating near-field BBA plumes from western US. The aging process can result in complex BBA structures and varying properties. Dahlkötter et al. (2014) sampled BBA particles in a 3-4 days old plume from western US wildfires in the UTLS. They found that a significant proportion of the particles are BC-containing particles mixed with light-scattering materials and the mixing state is highly varying. Observations of long-ranged transported Canadian smoke in 2017 and Australian smoke in 2019-2020 in UTLS showed enhanced particle linear depolarization ratios (PLDR) that had never been detected in tropospheric smoke layers (Haarig et al., 2018; Hu et al., 2019; Ohneiser et al., 2020; Khaykin et al., 2020). Similar signatures of PLDRs have also been observed in aged tropospheric BBAs originated from wildfires (Murayama et al., 2004; Burton et al., 2015). Researchers thought such characteristics of PLDRs are indications of complicated BBA particle morphology and effects of longtime aging. Since then, many efforts have been made to simulate aged BBA particles' optical properties. The simulations indicate that aerosol properties, such as the absorption and PLDRs, are strongly dependent on the morphology, mixing state and fractions of different components.

BBAs contribute to ice nucleating (IN) mainly through immersion freezing, contact freezing , deposition freezing, as well as pore condensation and freezing(Kanji et al., 2011; Umo et al., 2015; Grawe et al., 2016; Kanji et al., 2017; Knopf et al., 2018; Umo et al., 2019). These mechanisms are not yet well resolved and data about the onset condition of ice nucleation by BBA particles are diverse. As wildfire emissions become a more and more important atmospheric aerosol source, the role of BBAs as INP becomes increasingly important and different theories have been proposed to understand BBAs' IN ability. One important argument is that the amorphous state of organic matter and complicated morphology of BBAs at atmospheric conditions could influence the ability of water diffusion, thus causing strong perturbations in the prediction of cloud formation (Berkemeier et al., 2014; Knopf et al., 2018). Recently, Jahn et al. (2020) reported a different mechanism. They claimed that the inorganic elements naturally present in biomass could be transformed by combustion process to minerals, which are very ice active over a wide range of temperatures. Studies also found that the aging process could potentially increase the capability of BBA in cloud formation (Lupi and Molinero, 2014; Jahl et al., 2021). Therefore, the characterization of BBA properties in light scattering and cloud formation after long-range transport is an important direction to improve the representation of aerosol model and further, the accuracy of the climate model.

The 2020 California wildfires are the largest in Californian modern history. They comprise about 9639 fire activities reported in the California state, located in the western coast of the United States. The fire season started from the beginning of May 2020. By the end of the year, nearly 10,000 fires had burned over 4.2 million acres, more than 4% of the state's roughly 100 million acres of land (https://www.fire.ca.gov/incidents/2020/). In mid-August, the first 'gigafire' spreading over 7 counties in northern California was recorded. 'Gigafire' is a level above 'megafire' and describes a blaze burning at least a million acres of land. Satellite observations indicated this fire activity caused huge BBA emissions over the middle and western US, while the plumes faded away after 1 week without being transported to other continents. In September 2020, the fire activities revived after a short pause. Fire emissions were lofted into UTLS by high winds or convective pyro-cumulonimbus, and then transported to Europe by the prevailing westerlies (Baars et al., 2021). The densest smoke plumes detected at the observatory ATOLL (ATmospheric Observatory of LiLle) in Lille, France, is in the period of 10-23 September. In this study, we analyzed

the observations from multiple instruments and the optical properties derived from a multi-wavelength Mie-Raman polarization lidar equipped with a fluorescence channel.

2 Observations

2.1 Satellite observations – OMPS and CALIPSO

According to satellite observations, the smoke plumes detected in Lille on 10-22 September are attributed to the fire activities on 04-11 September in California and Oregon state in the USA. On 04-06 September 2020, the Creek fire started in the southwestern California. On 05 September, the fires generated a pyro-cumulonimbus (PyroCb) cloud reaching about 16000 m, S3
which might be the highest PyroCb cloud ever (Creek Fire, 2020). The plumes from Creek fire can be clearly seen in the earth's true color image (Figure 1(a)) and the maps of the UVAI from OMPS observations shown in Supplementary information (SI). The center of the lofted plumes was at (37.7N, 117.8W) on 06 September and then transported rapidly toward the northeast. On 07-10 September, the forest in the west coast of California and Oregon started to burn, which will be called Oregon fires hereafter (Oregon Fire, 2020). The burning area was in serious drought and under the blasts of fierce winds, which lifted vast fire emissions into the atmosphere. On 09 September, the wind whipped up fires and generated a pyro-cumulus cloud. Due to cyclone activities, the plumes were trapped on the eastern Pacific ocean and west coast of the US on 07-11 September, as shown in Figure 1(b). The plumes started spreading on 12 September and arrived in Europe on 16-18 September.
S4,S5
Figure 2 shows the CALIPSO observations in the transport pathway. The plumes in Figure 2(a, b, c) and in Figure 2(d, e, f) are attributed to the Creek fire and the Oregon fire, respectively. The plume origins were identified using HYSPLIT back trajectories and OMPS UVAI maps, shown in SI. The plumes emitted by the Creek fires are mostly classified as 'elevated smoke' by the CALIPSO aerosol typing algorithm (Version 4.21), while the plumes emitted from Oregon fires are mostly detected as 'polluted dust'. The reason is that the particle linear depolarization ratio (PLDR) at 532 nm of the BBA particles from Oregon fire was higher than Creek fire. PLDR is a parameter reflecting the particle shape, i.e. spherical particles have PLDR of zero while morphologically complicated particles such as dust and ice crystals have high PLDRs. $PLDR_{532}$ is about 0.02–0.05 in Creek plume after 3–7 days' transport in the upper troposphere. In comparison, the $PLDR_{532}$ in Oregon plume is about 0.10–0.15 after 1–7 days' transport. The observed differences of BBA properties in the two events may be attributed to the combustion and lifting process.

2.2 Sun/sky photometer observations near wildfire source

NASA_Ames and PNNL are two AERONET sites located near the fire activities, as shown in Figure 1(b). PNNL was mainly impacted by the Oregon smoke during 12–19 September. S4,S5
In Figure 3, the AOD_{500} (Aerosol Optical Depth at 500 nm) was about 0.2 and $AE_{340-500}$ (Angström exponent between 340 and 500 nm) about 1.5 on 01–08 September, before the arrival of the Oregon smoke. When the Oregon plumes arrived at PNNL on 12 September, the AOD sharply increased and the AE decreased at the same time. The AOD_{500} significantly increased and the maximal AOD_{500} was about 4.0, with corresponding

$AE_{340-500}$ of 0.2, during 12-19 September. NASA_Ames is in the west of the Creek fire and was influenced firstly by the Creek fire and then by the Oregon fire. AOD_{500} on 04–08 September, when Creek smoke particles dominated, was less than 1.0 (with $AE_{340-500}$ ~1.2), because the center of the Creek plumes propagated eastward and only a part of it drifted to the west. The Oregon plumes started on 09 September, as indicated by a sharp increase of AOD and a decrease of $AE_{340-500}$. The peak AOD_{500} of 5.8, corresponding to $AE_{340-500}$ ~0.0, was detected on 12 September in NASA_Ames. Similar to the observation at PNNL, $AE_{340-500}$ obviously decreased during the episodes of Oregon smoke. The decrease of $AE_{340-500}$ indicates the increase of particle size in the Oregon BBA plumes, which is in agreement with the CALIPSO observations. S6

2.3 Lidar and photometer observations in Lille, France

The lidar involved in this study is a multi-wavelength Mie-Raman-polarization-fluorescence lidar, LILAS, operated at ATOLL platform, University of Lille, France. The lidar system uses a Nd: YAG laser and has three emitting wavelengths, i.e., 355, 532 and 1064 nm. The backscattered lidar signals are collected at three elastic wavelengths each coupled with a parallel channel and a cross channel, and three Raman channels at 387 (vibrational Raman of N_2 and O_2), 530 (rotational Raman of N_2 and O_2) and 408 nm (water vapor channel). In December 2019, the water vapor channel was replaced by a fluorescence channel centered at 466 nm (excitation wavelength: 355 nm) in order to profile atmospheric fluorescence. A full description of this configuration and the results of the feasibility test can be found in Veselovskii et al. (2020). With this configuration, we can derive the height-resolved dataset $2\alpha + 3\beta + 3\delta + \phi$ (α: extinction coefficient, β: backscattering coefficient, δ: particle linear depolarization ratio, ϕ: fluorescence capacity). The fluorescence signal is attributed to certain molecules that could absorb in the incident laser light and re-emit it at longer wavelengths. The fluorescence capacity represents the capacity of aerosol particles in producing fluorescence, hence it is linked to particle chemical compositions. Equation 1 and 2 demote respectively the fluorescence backscattering coefficient $\beta_F(z)$ and the fluorescence capacity $\phi(z)$.

S1

$$\beta_F(z) = \frac{C_R}{C_F}\frac{P_F(z)}{P_R(z)}\frac{T_R(z)}{T_F(z)}N_R(z)\sigma_R, \quad \text{S2} \tag{1}$$

where $P_F(z)$ and $P_R(z)$ are the lidar signals of fluorescence and Raman channel, respectively, $\frac{C_R}{C_F}$ is the ratio of instrumental constant between the Raman and the fluorescence channel and it is determined by calibration. $N_R(z)$ is the vertically distributed number concentration of Raman scatters (i.e., N_2 and O_2) and σ_R is the Raman differential scattering cross section in the backward direction. With β_F, one can define the fluorescence capacity $\phi(z)$:

$$\phi(z) = \frac{\beta_F(z)}{\beta_{\lambda_0}(z)}. \quad \text{S2} \tag{2}$$

S2

According to our observations, BBA and pollen particles are very efficient in producing fluorescence, while dust particles and continental aerosols are much less efficient. More information about fluorescence lidar measurements and aerosol fluorescent signatures can be found in our previous publications (Hu et al., 2019; Veselovskii et al., 2020, 2021b).

Figure 4 shows lidar observations in the period of 11-22 September 2020. Figure 4(a) and 4(b) show the range corrected lidar signal and the volume depolarization ratio at 1064 nm, respectively. The background aerosols in Lille are usually low depolarizing fine particles in the boundary layer. During the observational period, the BBA layers distributed at 2000-14000

m and polluted dust in the boundary layer were the two aerosol species. The smoke plumes are obvious in Figure 4(a) and disappear in Figure 4(b), because BBA particles have very weak depolarization at 1064 nm. The most intense smoke plumes are observed on 11-12 September, corresponding to $AOD_{500} \approx 0.65$ and $AE_{340-500} \approx 0.70$, shown in Figure 4(c). Aerosols in the boundary layer on 14-16 September were strongly depolarizing. Back trajectories and modeling results indicated the cause for the enhanced depolarization could be polluted dust or transported pollen. On 17-18 September, a decrease of $AE_{340-500}$ is detected when a smoke plume appeared at 6000-10000 m. The AOD_{500} and $AE_{340-500}$ on 17 September are about 0.22 ± 0.02 and 0.0 ± 0.20, respectively.

Figure 5 plots the intensive parameters in the BBA layers detected in time intervals in September 2020. The observation time and the height range of the layers are presented in Table 1. Lidar ratio, i.e., the ratio between extinction coefficient and backscatter coefficient, is correlated with multiple factors, such as the particle shape, size and refractive indices. LR_{355} being lower than LR_{532} is a typical feature of aged smoke particles from North America and Siberian wildfires. The values of lidar ratios varied in the range of 20–50 sr at 355 nm and 42-90 sr at 532 nm. The spectral dependence of the PLDRs is in agreement with the aged wildfire smoke particles in the literature. The variation ranges of PLDRs are respectively 0.03–0.22, 0.02–0.16 and 0.01–0.03 at 355, 532 and 1064 nm in the investigated cases. The PLDRs on 18 and 19 September (P7 and P8) are higher than other days, with mean PLDR equals 0.16 at 355 nm, 0.12 at 532 nm and 0.02 at 1064 nm. The fluorescence capacity varied from 1.0×10^{-4} to 4.0×10^{-4}. The $BAE_{355-532}$ (Angström exponent related to backscatter coefficient) is in the range of 1.5–2.5. Whereas, the variation of $EAE_{355-532}$ (Angström exponent related to extinction coefficient) is stronger. Before 17 September, the $EAE_{355-532}$ varied in the range 0.5-1.5 and after this day, it dropped to below zero. The vertical variations in the BBA layers, indicated by the distance between the bottom and the top of each box plot in Figure 5, are also significant, such as lidar ratios on 12 and 14 September, the PLDRs on 11 and 18 September. Such variations are possibly indications of the variabilities in the burning materials, combustion conditions, convective lifting and aging process. Two events corresponding to Creek fire and Oregon fire, respectively, are selected and analyzed in detail in next section.

F7

3 Case study

3.1 Case 1: 11-12 September 2020

The BBA plumes detected on the night of 11-12 September 2020 are attributed to the Creek fire and have traveled about 5-7 days. Figure 6(a) shows the 4-day back trajectories overlaid with UVAI map on 8 September 2020. Two areas with intense UVAI are indicated on the map, one over the western coast of the US and the other one over the Great Lakes. The former was mostly generated by the Oregon fire, which started on 7 September. The latter was emitted by the Creek fire on 4-6 September and transported to Europe via an 'expressway'. Figure 7 shows the range corrected lidar signal (RCS) and volume linear depolarization ratio (VLDR) and calibrated signal ratio between 466 and 387 nm channel, i.e., $\frac{C_R P_{466}(z)}{C_F P_{387}(z)}$. The fluorescence observations are only available at nighttime when there is no sunlight interference. The BBA layer was mainly distributed at 5000-10000 m and was characterized by strong fluorescence. In Figure 7(b), ice particles featured with increased depolariza-

S3

tion ratios were detected within high smoke layers, for example, at 8000-10000 m at 17:00–18:00 UTC. S4

Figure 8 plots the parameters obtained from averaged observations between 22:00 UTC, 11 September and 03:00 UTC, 12 September. The extinction coefficients peaked at about 6200 m, with 180 Mm^{-1} at 355 nm and 140 Mm^{-1} at 532 nm. The $EAE_{355-532}$ was about 0.5±0.3 and the $BAE_{355-532}$ was about 2.0±0.3. The $EAE_{355-532}$ is lower than the $AE_{340-500}$ measured at NASA_Ames when influenced by the Creek fire plumes, indicating the particle growth during the aging process. The lidar ratios, which are 40±6 sr at 355 and 70±11 sr at 532 nm, are typical values of aged smoke particles (Haarig et al., 2018; Hu et al., 2019; Ohneiser et al., 2020; Peterson et al., 2018). The PLDRs show strong vertical variations in the BBA layer. In the core of the smoke, i.e., 5000-6000 m, the PLDRs at the three wavelengths are all below 0.03. In the plume edge, i.e., 6500-9000 m, the PLDRs at 355 and 532 nm increased significantly, with about 0.15±0.03 at 355 nm and 0.12±0.02 at 532 nm. $PLDR_{1064}$ shows no significant vertical variations. A slight decreasing trend in the $EAE_{355-532}$ and a moderate one in $BAE_{355-532}$ are observed when the height increases. BBA particles at 5000-6000 m was also characterized with stronger fluorescence capacity ($\sim 3.8\times10^{-4}$) compared to those at 6500-9000 m. According to laboratory studies, the main fluorophores in smoke are the humic-like substance and PAHs (Garra et al., 2015; Zhang et al., 2019), which are common products of the combustion of biomass, as well as some SOA formed in the aging process (Lee et al., 2013). Therefore, temporal and spatial variations of fluorescence capacity are very likely during the transport, and such variation is controlled by factors, such as oxidation and evaporation of some chemical species and so on.

S5

Figure 8(g) presents the WVMR (water vapor mixing ratio) and RH (relative humidity) profiles measured by radio sounding at Beauvechain station (Belgium), 120 km to ATOLL platform. The RH with respect to ice (RH_{ice}) was calculated with the radio sounding measurements (Jarraud, 2008). The presence of the BBA layer is well reflected by the enhanced values in the WVMR profile. It indicates that the BBA plumes were also captured by the radio sounding measurements at Beauvechain due to the plumes' large spatial coverage. The WVMR in the core of the plume is obviously higher than at the plume edge, suggesting that the WVMR is an important factor in the agin process.

S6

3.2 Case 2: 17-18 September 2020

The smoke layers at 5000-9000 m on 17-18 September 2020 (Figure 9) are attributed to the Oregon fire, as shown in Figure 6(b). The plumes covered large areas of America and eastern Pacific Ocean and underwent 7-12 days of transport before arriving at the observation site ATOLL, France.

Profiles obtained from averaged measurements between 22:30 UTC, 17 September and 03:00 UTC, 18 September are plotted in Figure 10. Compared to Case 1, BBA plumes in Case 2 have lower extinction coefficients, $EAE_{355-532}$, lidar ratios and higher PLDRs. The $EAE_{355-532}$ is around -0.30±0.30, obviously lower than in Case 1. It can be explained by the longer travel time in Case 2, making the BBA particles bigger. Particle growth during transport has been reported in previous aged smoke observations (Müller et al., 2007; Hu et al., 2019; Bian et al., 2020). The lidar ratios are 24±4 sr at 355 nm and 50±8 sr at 532 nm, lower than the values in Case 1 and in most previous studies (Haarig et al., 2018; Hu et al., 2019; Ohneiser et al., 2020). Such low lidar ratios were detected by Ortiz-Amezcua et al. (2017) in long-range transported North America smoke over two European lidar stations, Leipzig (Germany) and Granada (Spain). The observations in Ortiz-Amezcua et al. (2017)

S8

showed mean $EAE_{355-532}$ of 0.2-0.3, and mean lidar ratios of 23-25 sr at 355 nm and 47-51 sr at 532 nm. PLDRs in Case 2 are 0.15±0.03 to 0.18±0.04 at 355 nm, 0.12±0.02 to 0.14±0.03 at 532 nm and about 0.02 at 1064 nm, higher than those in Case 1, especially at shorter lidar wavelengths. The fluorescence capacity varied in 2.0-2.8$\times 10^{-4}$ at 5300-8000 m, which is 26-47% lower than that plume core, and comparable with that in the plume edge in Case 1. This decrease of fluorescence capacity may be linked to the evaporation of organic species when the BBA plumes is diluted during the transport (Hodshire et al., 2021).

In Figure 10(e), a sharp increase of $PLDR_{1064}$ to nearly 0.10 was detected at 8600 m, indicating the presence of ice crystals. S7
At such altitude, the temperature was about -41°C to -34°C and the RH_{ice} was 100-120%, according to GDAS model data (GDAS: global data assimilation system) and radio sounding measurements. Lidar signals before and during the presence of cirrus have been averaged and shown in Figure 11. The fluorescence backscattering coefficient in the cirrus layer is as high as before the presence of ice crystals, indicating that the cirrus layer contains non-negligible BBA particles. This observation is an indication of BBA particles acting as INP, although the possibility that ice crystals formed elsewhere cannot be excluded. Considering that cloud coverage is quite low over northern France on 17-18 September, these ice crystals were very likely formed through deposition freezing mode or pore condensation and freezing mode (Cziczo et al., 2013; Umo et al., 2019).

4 Discussion

In this study, the PLDRs of BBA originated from wildfires showed obvious variations dependent on different fire activities, different altitudes and water vapor content of the BBA layers. BBAs originating from the Oregon fire generally had higher PLDRs than those from the Creek fire. Such a feature is probably due to the differences of burning vegetation type, combustion conditions and lifting process. During the episodes of transported Canadian smoke over Europe, lidar systems in Leipzig and Lille both found that the tropospheric BBA plumes had much lower PLDRs than the plumes simultaneously presenting in the UTLS (Haarig et al., 2018; Hu, 2018). In Case 1, the increase of PLDRs with altitude was observed in the BBA layer. This correlation between aged BBA PLDRs and altitude is likely driven by the altitude-dependent factors in the atmosphere, such as RH, temperature, etc., which influence the BBA particles' morphology in the aging process (Yu et al., 2019; Ohneiser et al., 2020; Ansmann et al., 2021). The organic aerosols, the main contributor of the BBA mass, can exist in amorphous state, in response to temperatures and RH (Koop et al., 2011; Berkemeier et al., 2014; Knopf et al., 2018). Studies demonstrated that the evaporation of condensed liquid water on the surface of BBA contributes strongly to the collapse of fractal-like aggregates into compact particles (Kütz and Schmidt-Ott, 1992; Ma et al., 2013). The concentration of BBA particles, which generally decrease during transport and aging, could also impact the evaporation and coagulation of particle aging, thus modifying the particles' morphology Hodshire et al. (2021). S9, S11

The lower lidar ratios detected in Case 2 of this study were rarely observed in previous lidar measurements. The decrease of lidar ratios in the Oregon plumes could be an indication of the decreased aerosol absorption, according to the modeling of aerosol optical properties (Gialitaki et al., 2020; Liu and Mishchenko, 2020). Different scattering models have been considered to understand how aerosol composition, morphology and mixing state influence BBA absorption. Liu and Mishchenko (2018) used 11 different morphology models, ranging from bare soot to completely embedded soot mixtures and found that the

absorption enhancement is affected by the particle size, morphology and the thickness of coating. Moreover, the combustion and aging process, as well as the environment conditions could also contribute to the variability of BBA absorption. More efforts in the characterization of wildfire emissions and the modeling of BBA scattering are required to answer this question.

The fluorescence signal brings new information for the characterization of aerosol properties. In previous studies we have shown that the fluorescence signal is a good reference for aerosol classification (Veselovskii et al., 2020, 2021b). In this study, we showed that the fluorescence capacity is correlated with the optical properties of BBA particles. As the fluorescence signal is attributed to certain chemical species, the variation of the fluorescence capacity directly reflects their abundance in BBAs, which is controlled by the combustion process, which determined their original concentration, and the aging process, consisting of complex processes, such as the oxidation, evaporation of versatile species, the condensation of gases and so on. For example, the decrease of fluorescence capacity at the plume edge in Case 1 is likely due to the evaporation of some fluorescence organic species when the BBA plume is diluted.

S9, S11

Handful studies have shown that BBAs may serve as INP (McCluskey et al., 2014; Jahn et al., 2020; Jahl et al., 2021), but existing results of ice nucleation onset conditions are highly variable. Laboratory studies on organic INPs are mostly limited to pure organics, such as sucrose and levoglucosan, etc., while OA in ambient conditions have complex origins. As a result, the conditions for initiating ice nucleation required by different organics are highly varying in literature data, which blocked us from clarifying the role of organic aerosols in ice formation (Kanji et al., 2017). Veselovskii et al. (2021a) presented that one can estimate the particle concentration even in thin aerosol layers using the fluorescence signal, which offers a new opportunity for the studies of aerosol-cloud interactions. A paper about the estimation of BBA surface concentration in freshly formed cirrus layers using fluorescence measurements collected at ATOLL platform has been presented in (Veselovskii et al., 2021a).

5 Conclusions

This study reported the observations of long-range transported BBA plumes originated from wildfires in North America in September 2020. After 1-2 weeks' transport, the emitted BBA plumes in the troposphere were detected by LILAS, a multi-wavelength Mie-Raman polarization fluorescence lidar in ATOLL, France. Our results confirmed the main typical features of aged BBA particles, i.e. the decreased Angström exponent after long-range transport, enhanced PLDRs at shorter wavelengths and lidar ratio at 532 nm greater than at 355 nm, that have been reported in previous research. Moreover, our results demonstrated that the properties of BBAs have strong variations. The PLDR varied from 0.03 (0.02) to 0.22 (0.16) at 355 (532) nm during the observations in September. Very specific lidar ratios, 24±4 sr at 355 nm and 50±8 sr at 532 nm, which are lower than most previous observations, were detected in the transported BBA plume from Oregon fire. These characteristics reflect that the BBA properties, such as morphology and absorption, are highly dependent on complex factors in the combustion (vegetation type, burning temperature, wind conditions, etc.) and aging process (humidities, temperature, etc.). These variations need to be resolved and should be considered in the representation of BBAs in the climate model. The fluorescence backscattering coefficient and fluorescence capacity turned to be useful and supplementary information for BBA characterization, due to the high sensitivity to the presence of fluorophores in BBAs. The fluorescence capacity allows for an efficient identification of BBA

S12

particles and the quantification of fluorescent aerosols at low concentration, as has been presented in Veselovskii et al. (2020). The fluorescence signal also opens the opportunity of study BBA particles inside cirrus clouds, as shown in this study and Veselovskii et al. (2021a). However, additional observations on different aerosol types and spectral fluorescence information are still needed to refine the study. A new fluorescence lidar with a more powerful laser and multiple fluorescence channels is now under development in order to advance the studies of aerosols and aerosol-cloud interactions. S12

Data availability. The data is available upon any request.

Author contributions. QH performed lidar measurements, developed the code for data analysis and wrote the manuscript. PG is the PI of the project, supervised the experiments and improved the manuscript. IV helped in data analysis and establishment of the scientific arguments. TP helped perform lidar measurements and is in charge of the maintenance, automatization and operation of lidar system.

Competing interests. The authors declare no competing interests.

Acknowledgements. We acknowledge the CaPPA project (Chemical and Physical Properties of the Atmosphere), funded by the ANR (French National Research Agency) through the PIA (Programme d'Investissement d'Avenir) under contract « ANR-11-LABX-0005-01 », the Regional Council « Hauts-de-France » and the FEDER (European Funds for Regional Economic Development). We also would like to thank the following organizations and individuals for the financial support and for sharing their data and expertise: Service National d'Observation PHOTONS/AERONET-EARLINET, ESA/QA4EO, AERONET (PIs of the sites involved in this study: Roy Johnson, Brent Holben, Philippe Goloub), CPER CLIMIBIO, Russian Science Foundation (project 21-17-00114) and Agora-LAB.

References

F1: all doi numbers are added.

Abel, S. J., Haywood, J. M., Highwood, E. J., Li, J., and Buseck, P. R.: Evolution of biomass burning aerosol properties from an agricultural fire in southern Africa, Geophysical Research Letters, 30, https://doi.org/10.1029/2003GL017342, 2003.

Alduchov, O. A. and Eskridge, R. E.: Improved Magnus Form Approximation of Saturation Vapor Pressure, Journal of Applied Meteorology and Climatology, 35, 601 – 609, https://doi.org/10.1175/1520-0450(1996)035<0601:IMFAOS>2.0.CO;2, 1996.

Ansmann, A., Riebesell, M., Wandinger, U., Weitkamp, C., Voss, E., Lahmann, W., and Michaelis, W.: Combined Raman elastic-backscatter lidar for vertical profiling of moisture, aerosol extinction, backscatter, and lidar ratio, Applied Physics B: Lasers and Optics, 55, 18–28, https://doi.org/https://doi.org/10.1007/BF00348608, 1992.

Ansmann, A., Ohneiser, K., Mamouri, R.-E., Knopf, D. A., Veselovskii, I., Baars, H., Engelmann, R., Foth, A., Jimenez, C., Seifert, P., and Barja, B.: Tropospheric and stratospheric wildfire smoke profiling with lidar: mass, surface area, CCN, and INP retrieval, Atmospheric Chemistry and Physics, 21, 9779–9807, https://doi.org/10.5194/acp-21-9779-2021, https://acp.copernicus.org/articles/21/9779/2021/, 2021.

Baars, H., Radenz, M., Floutsi, A. A., Engelmann, R., Althausen, D., Heese, B., Ansmann, A., Flament, T., Dabas, A., Trapon, D., Reitebuch, O., Bley, S., and Wandinger, U.: Californian Wildfire Smoke Over Europe: A First Example of the Aerosol Observing Capabilities of Aeolus Compared to Ground-Based Lidar, Geophysical Research Letters, 48, e2020GL092 194, https://doi.org/https://doi.org/10.1029/2020GL092194, https://agupubs.onlinelibrary.wiley.com/doi/abs/10.1029/2020GL092194, e2020GL092194 2020GL092194, 2021.

Berkemeier, T., Shiraiwa, M., Pöschl, U., and Koop, T.: Competition between water uptake and ice nucleation by glassy organic aerosol particles, Atmospheric Chemistry and Physics, 14, 12 513–12 531, https://doi.org/10.5194/acp-14-12513-2014, https://acp.copernicus.org/articles/14/12513/2014/, 2014.

Bian, Q., Ford, B., Pierce, J. R., and Kreidenweis, S. M.: A Decadal Climatology of Chemical, Physical, and Optical Properties of Ambient Smoke in the Western and Southeastern United States, Journal of Geophysical Research: Atmospheres, 125, e2019JD031 372, https://doi.org/https://doi.org/10.1029/2019JD031372, https://agupubs.onlinelibrary.wiley.com/doi/abs/10.1029/2019JD031372, e2019JD031372 2019JD031372, 2020.

Burton, S., Hair, J., Kahnert, M., Ferrare, R., Hostetler, C., Cook, A., Harper, D., Berkoff, T., Seaman, S., Collins, J., et al.: Observations of the spectral dependence of linear particle depolarization ratio of aerosols using NASA Langley airborne High Spectral Resolution Lidar, Atmospheric Chemistry and Physics, 15, 13 453–13 473, https://doi.org/10.5194/acp-15-13453-2015, 2015.

China, S., Mazzoleni, C., Gorkowski, K., Aiken, A. C., and Dubey, M. K.: Morphology and mixing state of individual freshly emitted wildfire carbonaceous particles, Nature Communications, 4, https://doi.org/10.1038/ncomms3122, https://doi.org/10.1038%2Fncomms3122, 2013.

China, S., Scarnato, B., Owen, R. C., Zhang, B., Ampadu, M. T., Kumar, S., Dzepina, K., Dziobak, M. P., Fialho, P., Perlinger, J. A., et al.: Morphology and mixing state of aged soot particles at a remote marine free troposphere site: Implications for optical properties, Geophysical Research Letters, 42, 1243–1250, https://doi.org/10.1002/2014GL062404, 2015.

Creek Fire: https://www.insider.com/california-wildfires-generate-their-own-weather-via-thunderclouds-2020-9#:~:text=The%20particular%20pyrocumulonimbus%20cloud%20she,ever%20recorded%20in%20the%20US, last accessed: 2021-05-05, 2020.

Cziczo, D. J., Froyd, K. D., Hoose, C., Jensen, E. J., Diao, M., Zondlo, M. A., Smith, J. B., Twohy, C. H., and Murphy, D. M.: Clarifying the dominant sources and mechanisms of cirrus cloud formation, Science, 340, 1320–1324, https://doi.org/10.1126/science.1234145, 2013.

Dahlkötter, F., Gysel, M., Sauer, D., Minikin, A., Baumann, R., Seifert, P., Ansmann, A., Fromm, M., Voigt, C., and Weinzierl, B.: The Pagami Creek smoke plume after long-range transport to the upper troposphere over Europe–aerosol properties and black carbon mixing state, Atmospheric Chemistry and Physics, 14, 6111–6137, https://doi.org/10.5194/acp-14-6111-2014, 2014, 2014.

Ditas, J., Ma, N., Zhang, Y., Assmann, D., Neumaier, M., Riede, H., Karu, E., Williams, J., Scharffe, D., Wang, Q., et al.: Strong impact of wildfires on the abundance and aging of black carbon in the lowermost stratosphere, Proceedings of the National Academy of Sciences, 115, E11 595–E11 603, https://doi.org/10.1073/pnas.1806868115, 2018.

Garofalo, L. A., Pothier, M. A., Levin, E. J., Campos, T., Kreidenweis, S. M., and Farmer, D. K.: Emission and evolution of submicron organic aerosol in smoke from wildfires in the western United States, ACS Earth and Space Chemistry, 3, 1237–1247, https://doi.org/10.1021/acsearthspacechem.9b00125, 2019.

Garra, P., Maschowski, C., Liaud, C., Dieterlen, A., Trouvé, G., Le Calvé, S., Jaffrezo, J.-L., Leyssens, G., Schönnenbeck, C., Kohler, S., et al.: Fluorescence microscopy analysis of particulate matter from biomass burning: Polyaromatic Hydrocarbons as Main Contributors, Aerosol Science and Technology, 49, 1160–1169, https://doi.org/10.1080/02786826.2015.1107181, 2015.

Gialitaki, A., Tsekeri, A., Amiridis, V., Ceolato, R., Paulien, L., Kampouri, A., Gkikas, A., Solomos, S., Marinou, E., Haarig, M., et al.: Is the near-spherical shape the "new black" for smoke?, Atmospheric Chemistry and Physics, 20, 14 005–14 021, https://doi.org/10.5194/acp-20-14005-2020, 2020.

Grawe, S., Augustin-Bauditz, S., Hartmann, S., Hellner, L., Pettersson, J. B. C., Prager, A., Stratmann, F., and Wex, H.: The immersion freezing behavior of ash particles from wood and brown coal burning, Atmospheric Chemistry and Physics, 16, 13 911–13 928, https://doi.org/10.5194/acp-16-13911-2016, https://acp.copernicus.org/articles/16/13911/2016/, 2016.

Haarig, M., Engelmann, R., Ansmann, A., Veselovskii, I., Whiteman, D. N., and Althausen, D.: 1064 nm rotational Raman lidar for particle extinction and lidar-ratio profiling: cirrus case study, Atmospheric Measurement Techniques, 9, 4269–4278, https://doi.org/10.5194/amt-9-4269-2016, 2016.

Haarig, M., Ansmann, A., Baars, H., Jimenez, C., Veselovskii, I., Engelmann, R., and Althausen, D.: Depolarization and lidar ratios at 355, 532, and 1064 nm and microphysical properties of aged tropospheric and stratospheric Canadian wildfire smoke, Atmospheric Chemistry and Physics, 18, 11 847–11 861, https://doi.org/10.5194/acp-18-11847-2018, 2018.

Hodshire, A. L., Ramnarine, E., Akherati, A., Alvarado, M. L., Farmer, D. K., Jathar, S. H., Kreidenweis, S. M., Lonsdale, C. R., Onasch, T. B., Springston, S. R., et al.: Dilution impacts on smoke aging: evidence in Biomass Burning Observation Project (BBOP) data, Atmospheric Chemistry and Physics, 21, 6839–6855, https://doi.org/10.5194/acp-21-6839-2021, 2021.

Hu, Q.: Advanced aerosol characterization using sun/sky photometer and multi-wavelength Mie-Raman lidar measurements, Ph.D. thesis, Lille 1, www.theses.fr/2018LILUR078/document, 2018.

Hu, Q., Goloub, P., Veselovskii, I., Bravo-Aranda, J.-A., Popovici, I. E., Podvin, T., Haeffelin, M., Lopatin, A., Dubovik, O., Pietras, C., et al.: Long-range-transported Canadian smoke plumes in the lower stratosphere over northern France, Atmospheric Chemistry and Physics, 19, 1173–1193, https://doi.org/10.5194/acp-19-1173-2019, 2019.

Jahl, L. G., Brubaker, T. A., Polen, M. J., Jahn, L. G., Cain, K. P., Bowers, B. B., Fahy, W. D., Graves, S., and Sullivan, R. C.: Atmospheric aging enhances the ice nucleation ability of biomass-burning aerosol, Science Advances, 7, eabd3440, https://doi.org/10.1126/sciadv.abd3440, 2021.

Jahn, L. G., Polen, M. J., Jahl, L. G., Brubaker, T. A., Somers, J., and Sullivan, R. C.: Biomass combustion produces ice-active minerals in biomass-burning aerosol and bottom ash, Proceedings of the National Academy of Sciences, 117, 21 928–21 937, https://doi.org/10.1073/pnas.1922128117, 2020.

Jarraud, M.: Guide to meteorological instruments and methods of observation (WMO-No. 8), World Meteorological Organisation: Geneva, Switzerland, 29, https://doi.org/10.25607/OBP-1528, 2008.

Jolly, W. M., Cochrane, M. A., Freeborn, P. H., Holden, Z. A., Brown, T. J., Williamson, G. J., and Bowman, D. M.: Climate-induced variations in global wildfire danger from 1979 to 2013, Nature communications, 6, 1–11, https://doi.org/10.1038/ncomms8537, 2015.

Kanji, Z. A., DeMott, P. J., Möhler, O., and Abbatt, J. P. D.: Results from the University of Toronto continuous flow diffusion chamber at ICIS 2007: instrument intercomparison and ice onsets for different aerosol types, Atmospheric Chemistry and Physics, 11, 31–41, https://doi.org/10.5194/acp-11-31-2011, https://acp.copernicus.org/articles/11/31/2011/, 2011.

Kanji, Z. A., Ladino, L. A., Wex, H., Boose, Y., Burkert-Kohn, M., Cziczo, D. J., and Krämer, M.: Overview of Ice Nucleating Particles, Meteorological Monographs, 58, 1.1–1.33, https://doi.org/10.1175/AMSMONOGRAPHS-D-16-0006.1, https://doi.org/10.1175/AMSMONOGRAPHS-D-16-0006.1, 2017.

Khaykin, S., Legras, B., Bucci, S., Sellitto, P., Isaksen, L., Tencé, F., Bekki, S., Bourassa, A., Rieger, L., Zawada, D., Jumelet, J., and Godin-Beekmann, S.: The 2019/20 Australian wildfires generated a persistent smoke-charged vortex rising up to 35 km altitude, Communications Earth & Environment, 1, 22, https://doi.org/10.1038/s43247-020-00022-5, https://doi.org/10.1038/s43247-020-00022-5, 2020.

Kleinman, L. I., Sedlacek III, A. J., Adachi, K., Buseck, P. R., Collier, S., Dubey, M. K., Hodshire, A. L., Lewis, E., Onasch, T. B., Pierce, J. R., et al.: Rapid evolution of aerosol particles and their optical properties downwind of wildfires in the western US, Atmospheric Chemistry and Physics, 20, 13 319–13 341, https://doi.org/10.5194/acp-20-13319-2020, 2020.

Knopf, D. A., Alpert, P. A., and Wang, B.: The role of organic aerosol in atmospheric ice nucleation: a review, ACS Earth and Space Chemistry, 2, 168–202, https://doi.org/10.1021/acsearthspacechem.7b00120, 2018.

Koop, T., Bookhold, J., Shiraiwa, M., and Pöschl, U.: Glass transition and phase state of organic compounds: dependency on molecular properties and implications for secondary organic aerosols in the atmosphere, Phys. Chem. Chem. Phys., 13, 19 238–19 255, https://doi.org/10.1039/C1CP22617G, http://dx.doi.org/10.1039/C1CP22617G, 2011.

Kütz, S. and Schmidt-Ott, A.: Characterization of agglomerates by condensation-induced restructuring, Journal of aerosol science, 23, 357–360, https://doi.org/10.1016/0021-8502(92)90423-S, 1992.

Lee, H. J., Laskin, A., Laskin, J., and Nizkorodov, S. A.: Excitation–emission spectra and fluorescence quantum yields for fresh and aged biogenic secondary organic aerosols, Environmental science & technology, 47, 5763–5770, https://doi.org/10.1021/es400644c, 2013.

Liu, L. and Mishchenko, M. I.: Scattering and Radiative Properties of Morphologically Complex Carbonaceous Aerosols: A Systematic Modeling Study, Remote Sensing, 10, https://doi.org/10.3390/rs10101634, https://www.mdpi.com/2072-4292/10/10/1634, 2018.

Liu, L. and Mishchenko, M. I.: Spectrally dependent linear depolarization and lidar ratios for nonspherical smoke aerosols, Journal of Quantitative Spectroscopy and Radiative Transfer, 248, 106 953, https://doi.org/10.1016/j.jqsrt.2020.106953, 2020.

Lupi, L. and Molinero, V.: Does hydrophilicity of carbon particles improve their ice nucleation ability?, The Journal of Physical Chemistry A, 118, 7330–7337, https://doi.org/10.1021/jp4118375, 2014.

Ma, X., Zangmeister, C. D., Gigault, J., Mulholland, G. W., and Zachariah, M. R.: Soot aggregate restructuring during water processing, Journal of Aerosol Science, 66, 209–219, https://doi.org/10.1016/j.jaerosci.2013.08.001, 2013.

May, A., McMeeking, G., Lee, T., Taylor, J., Craven, J., Burling, I., Sullivan, A., Akagi, S., Collett Jr, J., Flynn, M., et al.: Aerosol emissions from prescribed fires in the United States: A synthesis of laboratory and aircraft measurements, Journal of Geophysical Research: Atmospheres, 119, 11–826, https://doi.org/10.1002/2014JD021848, 2014.

McCluskey, C. S., DeMott, P. J., Prenni, A. J., Levin, E. J., McMeeking, G. R., Sullivan, A. P., Hill, T. C., Nakao, S., Carrico, C. M., and Kreidenweis, S. M.: Characteristics of atmospheric ice nucleating particles associated with biomass burning in the US: Prescribed burns and wildfires, Journal of Geophysical Research: Atmospheres, 119, 10 458–10 470, https://doi.org/10.1002/2014JD021980, 2014.

Müller, D., Mattis, I., Ansmann, A., Wandinger, U., Ritter, C., and Kaiser, D.: Multiwavelength Raman lidar observations of particle growth during long-range transport of forest-fire smoke in the free troposphere, Geophysical Research Letters, 34, https://doi.org/10.1029/2006GL027936, 2007.

Murayama, T., Müller, D., Wada, K., Shimizu, A., Sekiguchi, M., and Tsukamoto, T.: Characterization of Asian dust and Siberian smoke with multi-wavelength Raman lidar over Tokyo, Japan in spring 2003, Geophysical Research Letters, 31, L23 103, https://doi.org/10.1029/2004GL021105, 2004.

O'Dell, K., Hornbrook, R. S., Permar, W., Levin, E. J., Garofalo, L. A., Apel, E. C., Blake, N. J., Jarnot, A., Pothier, M. A., Farmer, D. K., et al.: Hazardous air pollutants in fresh and aged western US wildfire smoke and implications for long-term exposure, Environmental Science & Technology, 54, 11 838–11 847, https://doi.org/10.1021/acs.est.0c04497, 2020.

Ohneiser, K., Ansmann, A., Baars, H., Seifert, P., Barja, B., Jimenez, C., Radenz, M., Teisseire, A., Floutsi, A., Haarig, M., et al.: Smoke of extreme Australian bushfires observed in the stratosphere over Punta Arenas, Chile, in January 2020: optical thickness, lidar ratios, and depolarization ratios at 355 and 532 nm, Atmospheric Chemistry and Physics, 20, 8003–8015, https://doi.org/10.5194/acp-20-8003-2020, 2020.

Oregon Fire: https://wildfiretoday.com/2020/09/10/wildfires-have-burned-over-800-square-miles-in-oregon/, last accessed: 2021-05-05, 2020.

Ortiz-Amezcua, P., Guerrero-Rascado, J. L., Granados-Muñoz, M. J., Benavent-Oltra, J. A., Böckmann, C., Samaras, S., Stachlewska, I. S., Janicka, Ł., Baars, H., Bohlmann, S., et al.: Microphysical characterization of long-range transported biomass burning particles from North America at three EARLINET stations, Atmospheric Chemistry and Physics, 17, 5931–5946, https://doi.org/10.5194/acp-17-5931-2017, 2017.

Peterson, D. A., Campbell, J. R., Hyer, E. J., Fromm, M. D., Kablick, G. P., Cossuth, J. H., and DeLand, M. T.: Wildfire-driven thunderstorms cause a volcano-like stratospheric injection of smoke, NPJ climate and atmospheric science, 1, 1–8, https://doi.org/10.1038/s41612-018-0039-3, 2018.

Reid, J. S., Koppmann, R., Eck, T. F., and Eleuterio, D. P.: A review of biomass burning emissions part II: intensive physical properties of biomass burning particles, Atmospheric Chemistry and Physics, 5, 799–825, https://doi.org/10.5194/acp-5-799-2005, https://acp.copernicus.org/articles/5/799/2005/, 2005.

Santín, C. and Doerr, S. H.: Fire effects on soils: the human dimension, Philosophical Transactions of the Royal Society B: Biological Sciences, 371, 20150 171, https://doi.org/10.1098/rstb.2015.0171, 2016.

Schoennagel, T., Balch, J. K., Brenkert-Smith, H., Dennison, P. E., Harvey, B. J., Krawchuk, M. A., Mietkiewicz, N., Morgan, P., Moritz, M. A., Rasker, R., et al.: Adapt to more wildfire in western North American forests as climate changes, Proceedings of the National Academy of Sciences, 114, 4582–4590, https://doi.org/10.1073/pnas.1617464114, 2017.

Umo, N. S., Murray, B. J., Baeza-Romero, M. T., Jones, J. M., Lea-Langton, A. R., Malkin, T. L., O'Sullivan, D., Neve, L., Plane, J. M. C., and Williams, A.: Ice nucleation by combustion ash particles at conditions relevant to mixed-phase clouds, Atmospheric Chemistry and Physics, 15, 5195–5210, https://doi.org/10.5194/acp-15-5195-2015, https://acp.copernicus.org/articles/15/5195/2015/, 2015.

Umo, N. S., Wagner, R., Ullrich, R., Kiselev, A., Saathoff, H., Weidler, P. G., Cziczo, D. J., Leisner, T., and Möhler, O.: Enhanced ice nucleation activity of coal fly ash aerosol particles initiated by ice-filled pores, Atmospheric Chemistry and Physics, 19, 8783–8800, https://doi.org/10.5194/acp-19-8783-2019, https://acp.copernicus.org/articles/19/8783/2019/, 2019.

Urbanski, S. P., Hao, W. M., and Baker, S.: Chemical composition of wildland fire emissions, Developments in environmental science, 8, 79–107, https://doi.org/10.1016/S1474-8177(08)00004-1, 2008.

Veselovskii, I., Hu, Q., Goloub, P., Podvin, T., Korenskiy, M., Pujol, O., Dubovik, O., and Lopatin, A.: Combined use of Mie–Raman and fluorescence lidar observations for improving aerosol characterization: feasibility experiment, Atmospheric Measurement Techniques, 13, 6691–6701, https://doi.org/10.5194/amt-13-6691-2020, 2020.

Veselovskii, I., Hu, Q., Ansmann, A., Goloub, P., Podvin, T., and Korenskiy, M.: Fluorescence lidar observations of wildfire smoke inside cirrus: A contribution to smoke-cirrus – interaction research, Atmospheric Chemistry and Physics Discussions, 2021, 1–29, https://doi.org/10.5194/acp-2021-1017, https://acp.copernicus.org/preprints/acp-2021-1017/, 2021a.

Veselovskii, I., Hu, Q., Goloub, P., Podvin, T., Choël, M., Visez, N., and Korenskiy, M.: Mie–Raman–fluorescence lidar observations of aerosols during pollen season in the north of France, Atmospheric Measurement Techniques, 14, 4773–4786, https://doi.org/10.5194/amt-14-4773-2021, https://amt.copernicus.org/articles/14/4773/2021/, 2021b.

Wu, G., Wan, X., Gao, S., Fu, P., Yin, Y., Li, G., Zhang, G., Kang, S., Ram, K., and Cong, Z.: Humic-like substances (HULIS) in aerosols of central Tibetan Plateau (Nam Co, 4730 m asl): Abundance, light absorption properties, and sources, Environmental science & technology, 52, 7203–7211, https://doi.org/10.1021/acs.est.8b01251, 2018.

Yu, P., Toon, O. B., Bardeen, C. G., Zhu, Y., Rosenlof, K. H., Portmann, R. W., Thornberry, T. D., Gao, R.-S., Davis, S. M., Wolf, E. T., de Gouw, J., Peterson, D. A., Fromm, M. D., and Robock, A.: Black carbon lofts wildfire smoke high into the stratosphere to form a persistent plume, Science, 365, 587–590, https://doi.org/10.1126/science.aax1748, https://doi.org/10.1126%2Fscience.aax1748, 2019.

Zhang, Y., Wang, L., Liu, P., Li, Y., Zhan, R., Huang, Z., and Lin, H.: Measurement and extrapolation modeling of PAH laser-induced fluorescence spectra at elevated temperatures, Applied Physics B, 125, 1–12, https://doi.org/10.1007/s00340-018-7115-6, 2019.

Table 1. The averaging time intervals and altitude ranges of selected BBA layers for the analysis of statistics. P1, P2, ... , P9 represent different time intervals in September 2020.

NO of period	Time interval [UTC]	Height [m]
P1	2020-09-11, 02:00:00 – 2020-09-11, 04:00:00	5500 – 7500
P2	2020-09-11, 22:00:00 – 2020-09-12, 03:00:00	5500 – 8500
P3	2020-09-12, 20:00:00 – 2020-09-12, 23:00:00	2500 – 3800
P4	2020-09-14, 00:00:00 – 2020-09-14, 03:00:00	5500 – 7500
P5	2020-09-14, 22:00:00 – 2020-09-15, 02:00:00	5500 – 6500
P6	2020-09-15, 02:00:00 – 2020-09-15, 04:00:00	4500 – 7200
P7	2020-09-17, 22:00:00 – 2020-09-18, 03:00:00	5400 – 8500
P8	2020-09-18, 20:00:00 – 2020-09-18, 22:00:00	4800 – 6500
P9	2020-09-20, 20:00:00 – 2020-09-21, 00:00:00	4400 – 6200

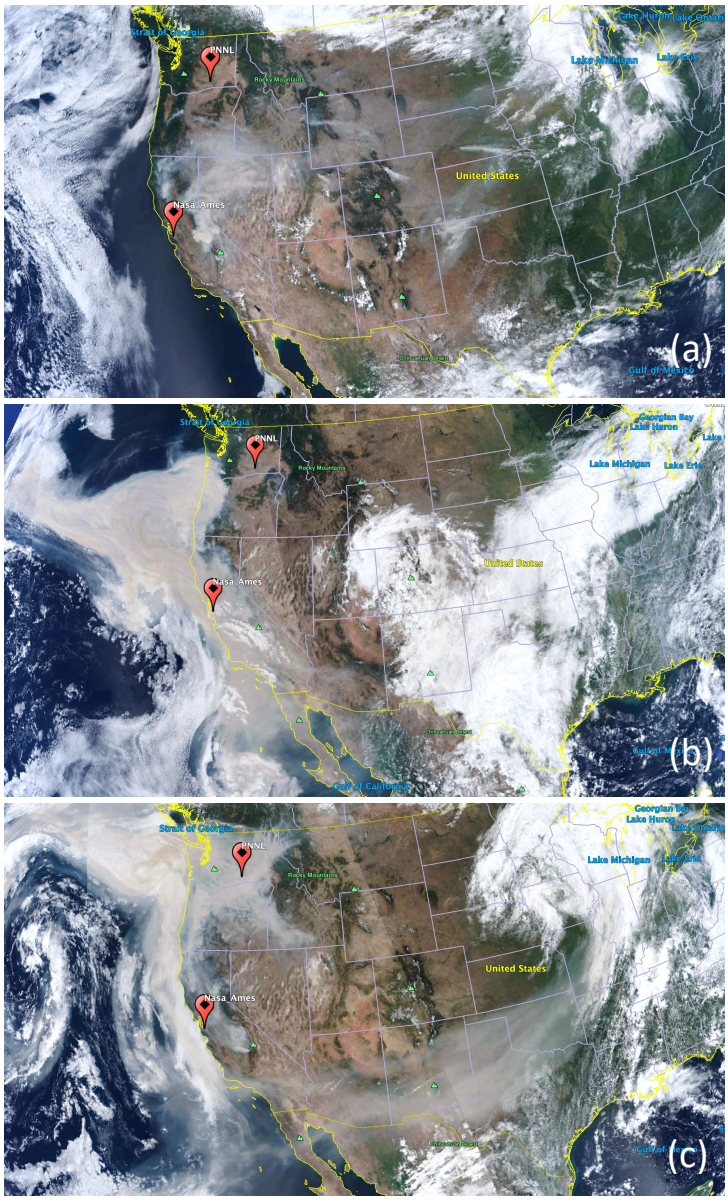

Figure 1. True color images from OMPS onboard Suomi NPP. (a) 06 September 2020, (b) 10 September 2020, (c) 12 September 2020. The two AERONET observation sites: NASA_Ames (37.420N, 122W) and PNNL (46N, 119W). ©Google Maps

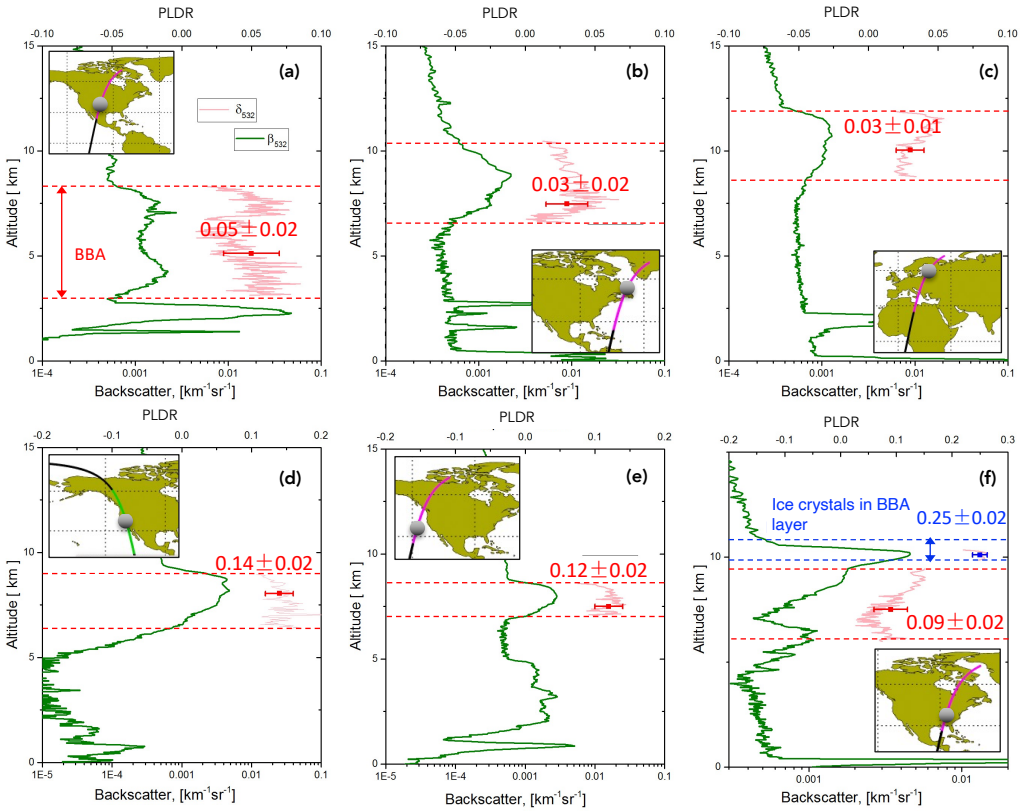

F6

Figure 2. The backscattering coefficients and PLDR ratio at 532 nm measured by CALIPSO. The smoke plumes in (a), (b) and (c) are attributed to Creek fires on 05-07 September 2020, and in (d), (e) and (f) are attributed to Oregon fires. The inserted maps display the granules of CALIPSO and the locations of the grey dots represent the region where the measurements are averaged. (a) Central US, 2020-09-08. (b) East of Quebec, 2020-09-09. (c) Eastern Europe, 2020-09-11. (d) Western coast of US, 2020-09-10. (e) Western coast of US, 2020-09-11. (f) Eastern US, 2020-09-14. The layer between the two red dashed lines is BBA. The blue dashed lines represent the location of the mixture of ice crystals and BBA particles.

F15

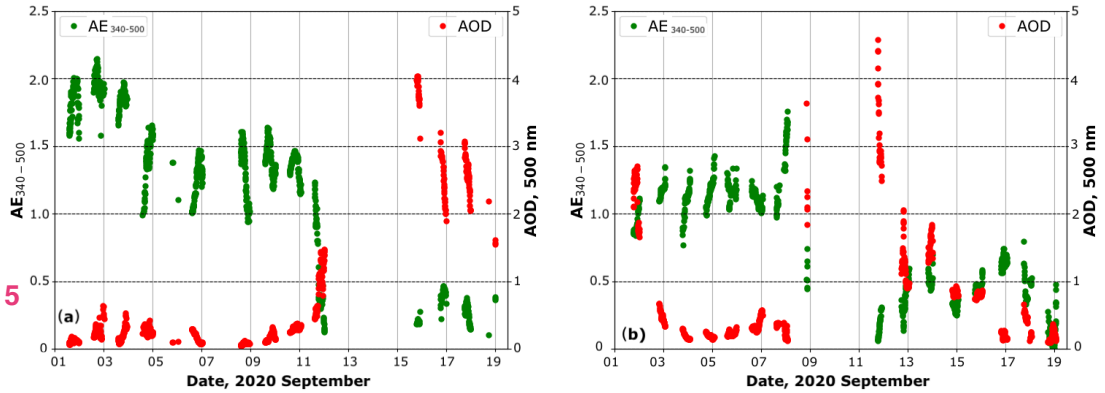

F6

Figure 3. AOD and AE (Level 1.5) measured by AERONET sun/photometers at two observation sites: (a) PNNL (46N, 119W) and (b) NASA_Ames (37.420N, 122W). NASA_Ames is within the influence of both the Creek fire and the Oregon fire. PNNL is mainly impacted by the smoke of Oregon fire. The smoke of Oregon fire arrived at NASA_Ames on about 9 September and at PNNL on 12 September 2020. The arrival of the Oregon smoke caused significant increase of AOD and decease of the AE at both sites.

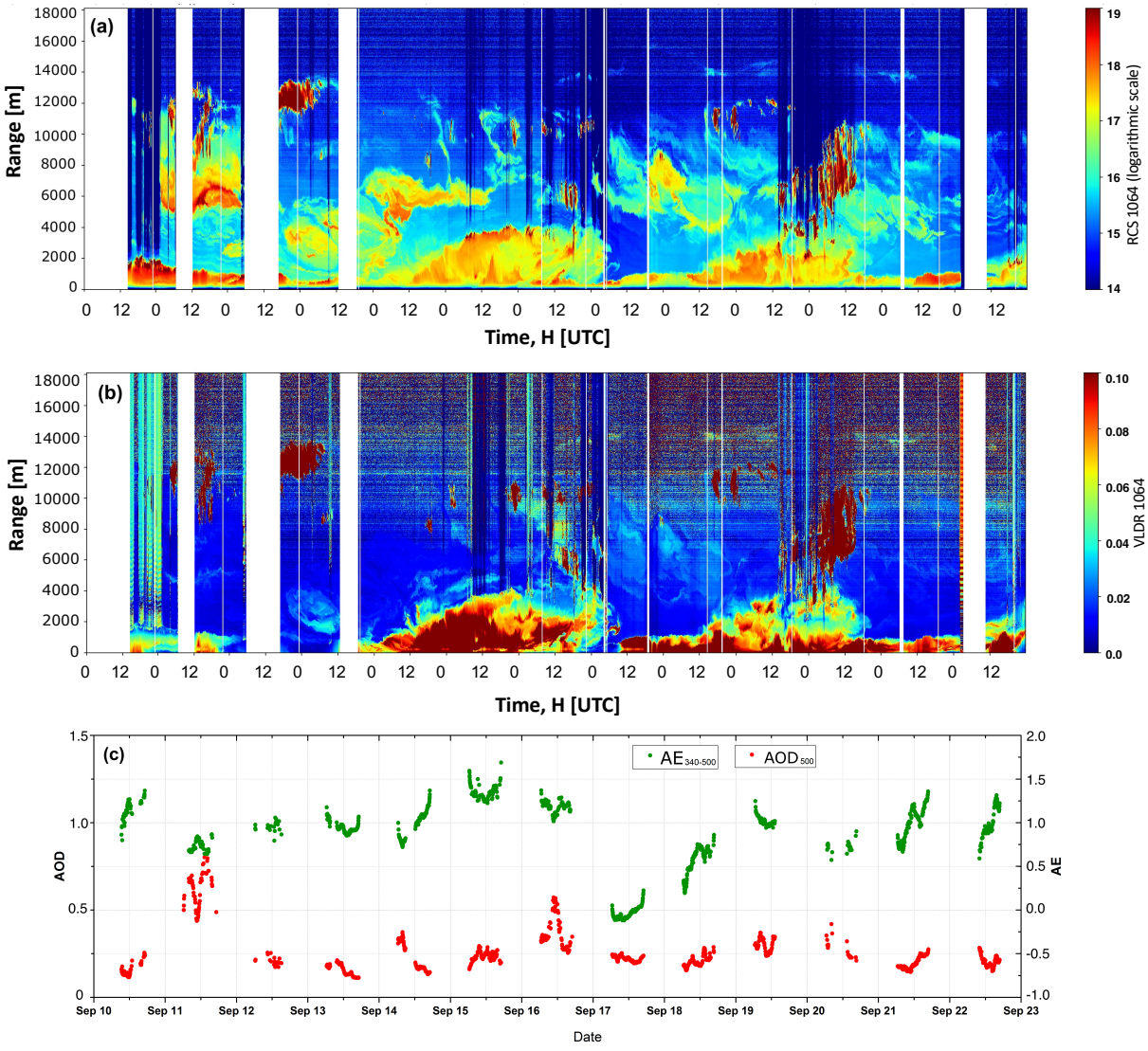

F15

Figure 4. Lidar and sun/sky photometer observations during the smoke episodes on 10-22 September 2020, ATOLL, France. (a) The range-corrected lidar signal at 1064 nm. (b) The volume depolarization ratio at 1064 nm. (c) The AOD and AE measured by the sun/sky photometer operated at ATOLL. The layers with strong depolarization appearing in the boundary layer on 14-16 September are polluted dust from Saharan region. The smoke layers from Californian smoke are mostly distributed in the free troposphere.

S14

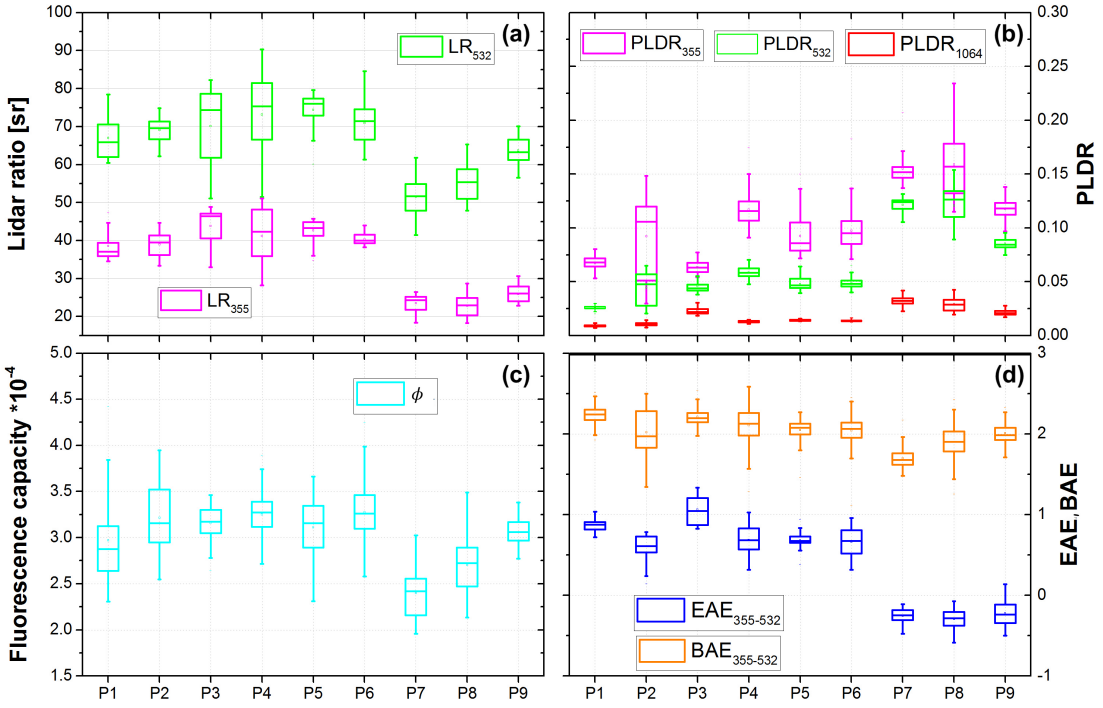

S15

F16, F17

Figure 5. Box plots of the variabilities of BBA intensive parameters during the smoke episodes in September 2020. P1, P2,..., P9 refer to the time intervals defined in Table 1. Only nighttime observations are considered in this analysis. The measurements in the time intervals are averaged The lower and upper edges of the box represents respectively the first and third quartiles of data. The lower and upper range-bars represent respectively the minimum and maximum. The dot and bar in the box indicate the mean value and the median value, respectively. (a) Lidar ratios, (b) PLDRs. The colors of the plots represent the different wavelengths (magenta: 355 nm, green: 532 nm, red: 1064 nm). (c) fluorescence capacity (in cyan), (d) $EAE_{355-532}$ (in blue) and $BAE_{355-532}$ (in orange).

S8

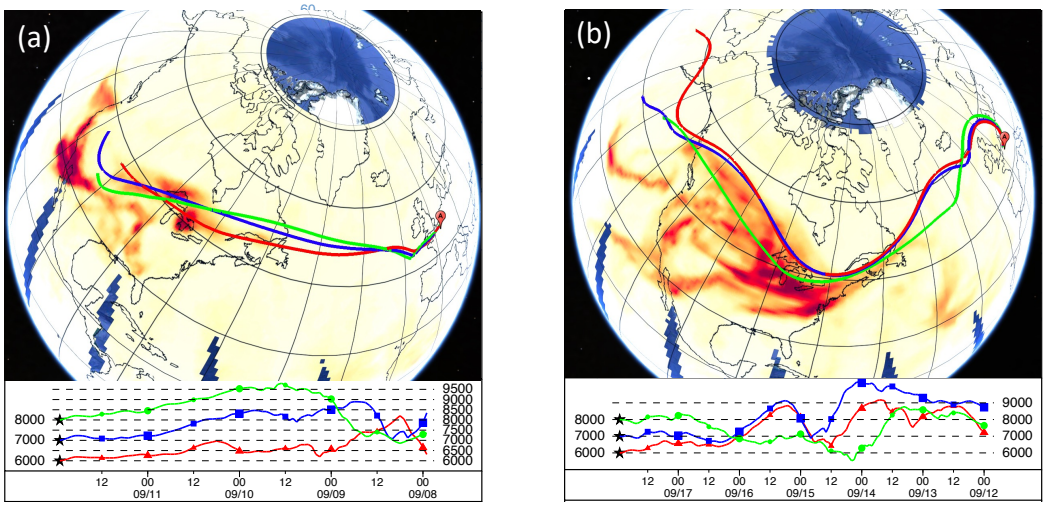

Figure 6. HYSPLIT back trajectories overlaid on the UVAI measured by OMPS onboard SUOMI-NPP satellite. (a) 96-hour back trajectories ending at 00:00 UTC, 12 September 2020 overlaid with UVAI on 08 September. (b)144-hour back trajectories ending at 00:00 UTC, 18 September 2020 overlaid with UVAI on 14 September. ©Google Earth.

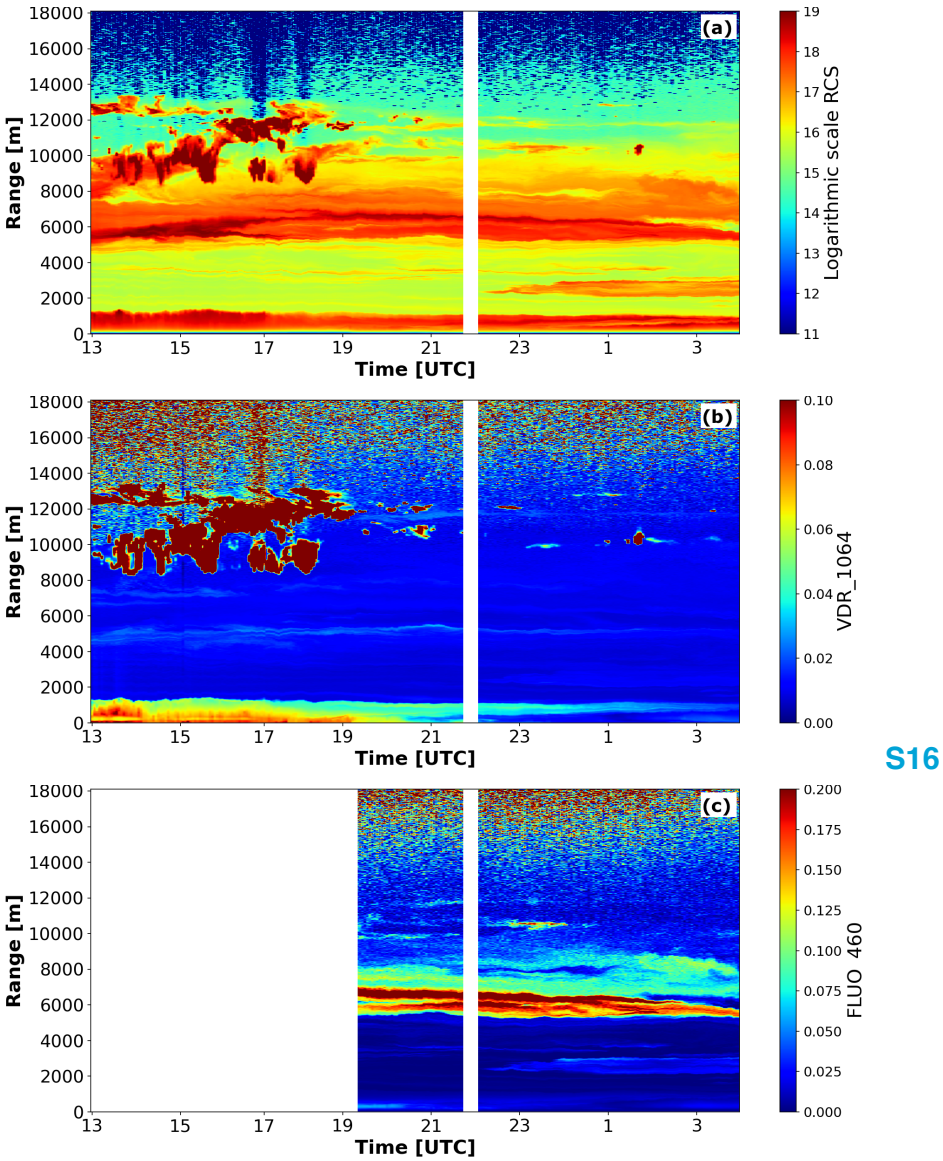

S16

Figure 7. Lidar observations on 11-12 September 2020. (a) Range corrected lidar signal at 1064 nm, (b) volume depolarization ratio at 1064 nm, (c) calibrated signal ratio between 466 and 387 nm channels, i.e. $\frac{C_R P_{466}}{C_F P_{387}}$ in Equation (1). This quantity is used as intermediate parameter to represent the fluorescence signal. The calibration coefficient C_R/C_F represents the ratio of the electro-optical gain between the 2 channels. The white zone in the figures represents missing data due to the turnoff of the detectors (ex. to avoid daytime sunlight interferences) or intermediate operations during the measurements.

S3

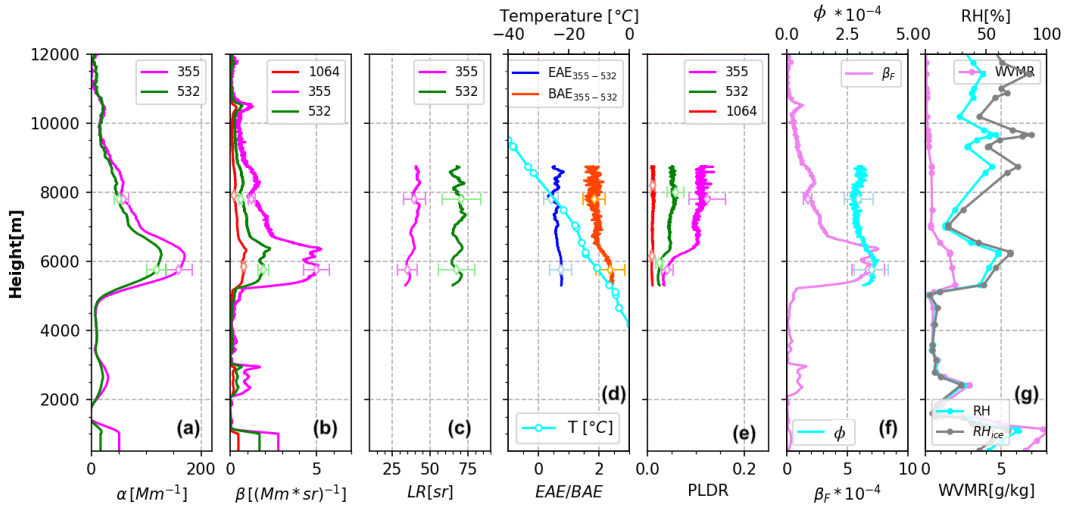

Figure 8. Aerosol vertical profiles from averaged measurements between 22:00, 11 September 2020 and 03:00, 12 September 2020, UTC. (a) Extinction coefficients, (b) backscattering coefficient, (c) lidar ratios. The colors of lines represent different wavelengths: 355 (magenta), 532 (green) and 1064 nm (red). (d) $EAE_{355-532}$ (orange), $BAE_{355-532}$ (blue) and temperature (cyan open circle), (e) PLDRs, (f) fluorescence backscattering coefficient (pink) and fluorescence capacity (cyan), (g) WVMR (pink solid circle), RH to liquid water (RH, pink solid circle) and ice (RH_{ice}, grey solid circle). The extinction and backscatter coefficients at 355 and 532 nm were calculated using Raman technique (Ansmann et al., 1992) and the backscatter coefficient at 1064 nm was calculated by Klett method with an assumption of LR=50 sr. The radio sounding station is in Beauvechain, Belgium, about 100 km from the lidar observation site. The error bars in the figure represent the statistical errors. The method of error estimation is presented in the Appendix of (Hu et al., 2019). The relative humidity to ice is calculated using the improved Magnus formula in Alduchov and Eskridge (1996). S5

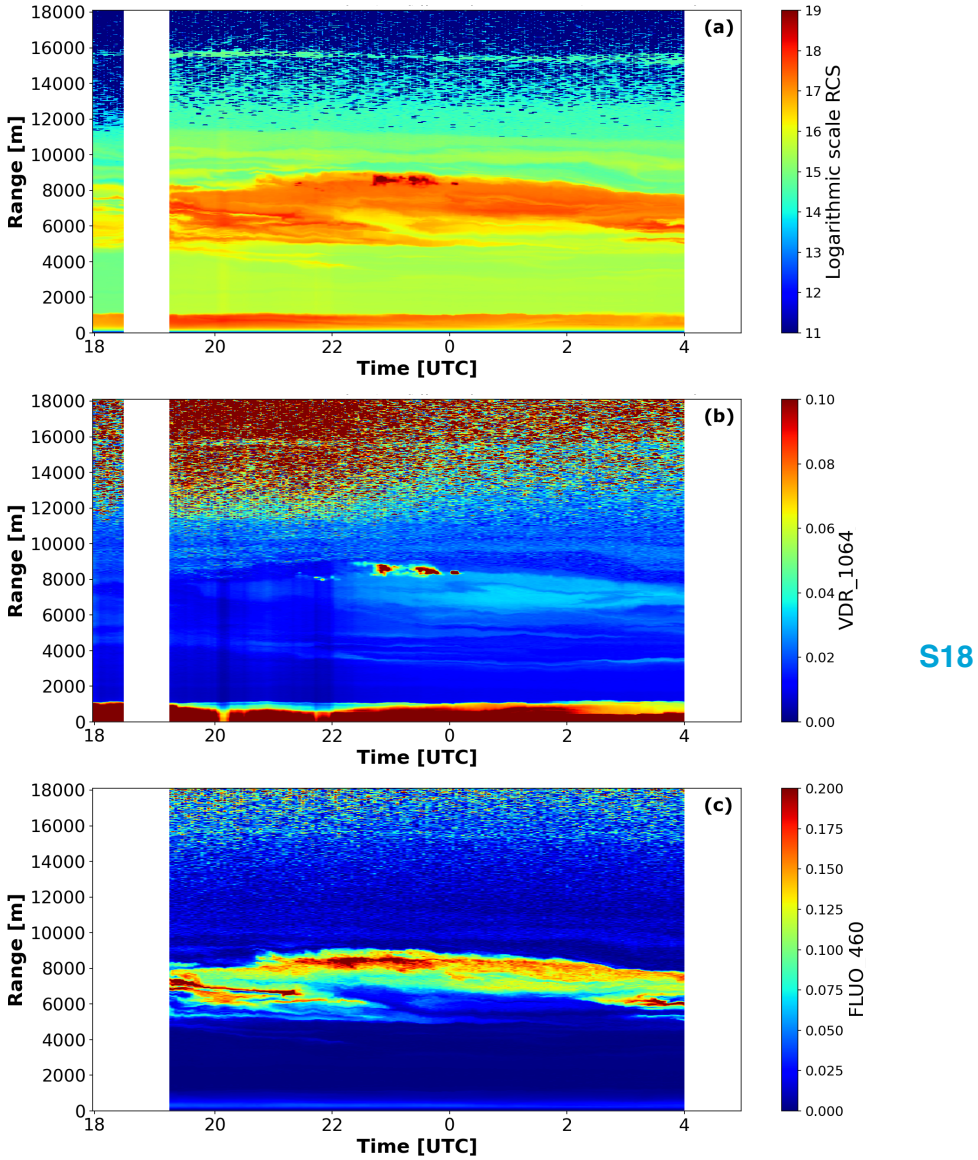

Figure 9. The same plot as Figure 7 but for lidar observation on 17-18 September 2020. (a) Range corrected lidar signal at 1064 nm, (b) volume depolarization ratio at 1064 nm, (c) calibrated signal ratio between 466 and 387 nm channels.

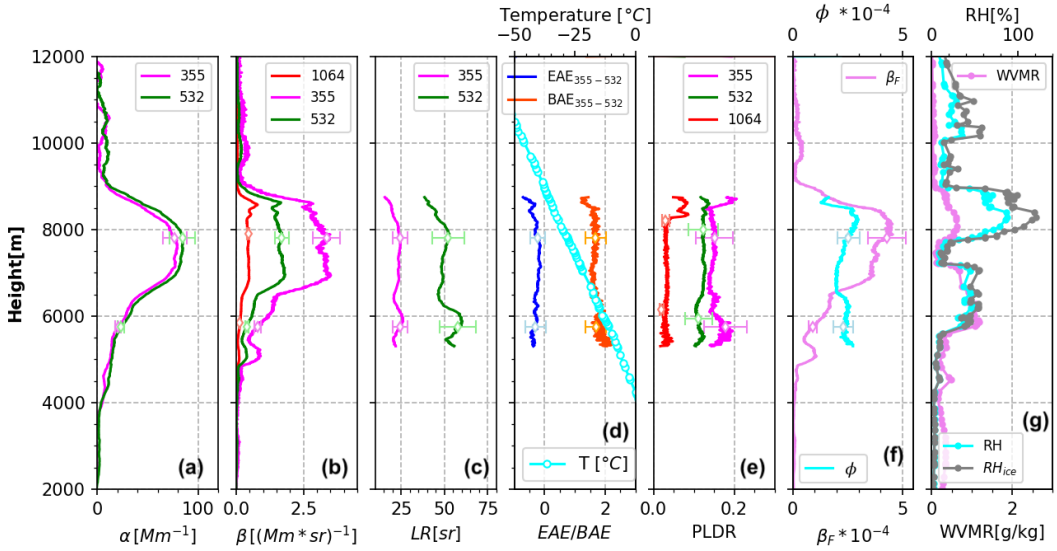

Figure 10. The same as Figure 8 except for observations between 22:30, 17 September 2020 and 03:00, 18 September 2020,UTC. The radio sounding measurements are from Hertzmonceux, England, which is about 200 km from the observation site. Radio sounding at Beauvecchain, Belgium is not available on this day.

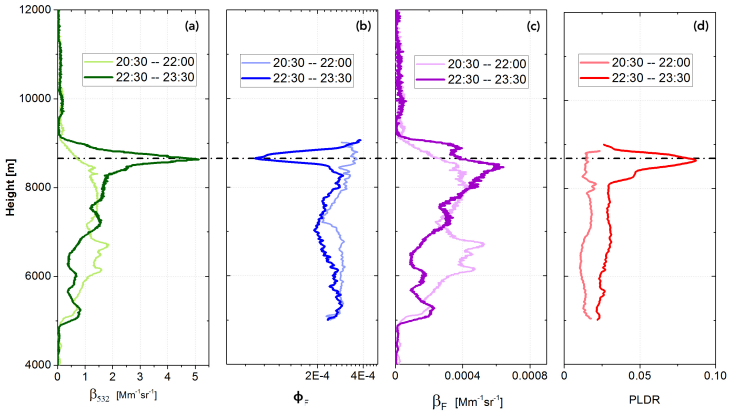

Figure 11. The profiles of averaged parameters in two consecutive periods: 20:30–22:30 UTC, 17 September 2020 (before the observation of ice crystals and in lighter colors) and 22:30–23:30 UTC, 17 September 2020 (during ice crystal observation and in darker colors). The dash-dotted line represents the altitude where the ice crystals appeared. (a) Backscattering coefficient at 532 nm, (b) fluorescence capacity at 466 nm, (c) fluorescence backscattering coefficient, (d) PLDR at 1064 nm.

S20